

Recursive anisotropy: A spatial taphonomic study of the Early Pleistocene vertebrate assemblage of Tsiotra Vryssi, Mygdonia Basin, Greece

D. Giusti^{a,*}, G. E. Konidaris^a, V. Tourloukis^a, M. Marini^b, M. Maron^b, A. Zerboni^b, N. Thompson^a, G. D. Koufos^c, D. S. Kostopoulos^c, K. Harvati^a

^a*Paläoanthropologie, Senckenberg Centre for Human Evolution and Palaeoenvironment, Eberhard Karls Universität Tübingen, Rümelinstr. 23, 72070 Tübingen, Germany*

^b*Università degli Studi di Milano, via Mangiagalli 34, 20133 Milano, Italy*

^c*Aristotle University of Thessaloniki, Department of Geology, Laboratory of Geology and Palaeontology, 54124 Thessaloniki, Greece*

Abstract

By applying advanced spatial statistical methods, spatial taphonomy complements the traditional taphonomic approach and enhances our understanding of biostratinomic and diagenetic processes. In this study, we elaborate on a specific aspect - spatial anisotropy - of taphonomic processes. We aim to unravel the taphonomic history of the Early Pleistocene vertebrate assemblage of Tsiotra Vryssi (Mygdonia Basin, Macedonia, Greece). Circular statistics are used for the fabric analysis of elongated elements; geostatistics (directional variograms), wavelet and point pattern analyses are applied for detecting anisotropy at the assemblage level. The anisotropy of magnetic susceptibility (AMS) of sedimentary magnetic minerals is as well investigated. The results of our analyses, integrated with preliminary remarks about the differential preservation of skeletal elements, sedimentological and micromorphological observations, suggest multiple dispersion events and recurrent spatial re-arrangement of a lag, (peri)autochthonous assemblage, consistent with the cyclical lateral switching of a braided fluvial system. Furthermore, this study offers an important contribution to the building of a spatial taphonomic referential framework for the interpretation of other fossil vertebrate assemblages, including archaeo-palaeontological ones.

*Corresponding author

Email address: domenico.giusti@uni-tuebingen.de (D. Giusti)

Keywords: Anisotropy, Spatial taphonomy, Taphonomy, Site formation processes, Early Pleistocene, Greece

1. Introduction

2 Since the first definition of taphonomy as “the study of the transition (in all its de-
3 tails) of animal remains from the biosphere into the lithosphere” ([Efremov, 1940](#)), the
4 spatial properties of taphonomic processes received special attention. Concerned about
5 thanatocoenosis, [Efremov \(1940\)](#) indicated as chief part of a taphonomic study, among
6 others, the analysis of “the spatial distribution of animal remains and their distribution
7 relatively to the planes of stratification”. More recent research on early hominid evo-
8 lution ([Behrensmeyer, 1975a](#); [Boaz and Behrensmeyer, 1976](#); [Hill, 1976](#)) extended the
9 original definition of taphonomy beyond its role as a “new branch of paleontology”
10 ([Efremov, 1940](#)) to include also formation and modification processes of the archae-
11 ological record. Despite some misrepresentations in the archaeological adaptation of
12 the original concept (e.g., the ontological difference between natural and cultural for-
13 mation processes; [Domínguez-Rodrigo et al., 2011](#); [Lyman, 2010](#)), in the last decades
14 taphonomy has widened its theoretical and methodological framework towards an inte-
15 grative and multidisciplinary investigation that aims to reconstruct the past in all its de-
16 tails, incorporating any signal of the processes, both natural and cultural, that modified
17 the original properties of the organic and inorganic components ([Domínguez-Rodrigo
et al., 2011](#)).

19 If taphonomy evolved towards an evolutionary and systemic approach that em-
20 braces multiple taphonomic levels of organisation (i.e., basic taphonomic elements,
21 taphonomic groups [taphons], taphonomic populations and taphoclades; [Fernández-
22 López, 2006](#)), likewise, the study of the spatial properties of taphonomic processes
23 extended from the analysis of the spatial distribution of animal remains in relation to
24 the stratigraphic setting, towards a multilevel quantitative investigation of the spatial
25 behaviour of different taphonomic entities (*sensu* [Fernández-López, 2006](#)). Therefore,
26 spatial taphonomy ([Domínguez-Rodrigo et al., 2017](#); [Giusti and Arzarello, 2016](#)), en-
27 compasses the spatial properties of basic entities (i.e., taphonomic elements, constitut-

28 ing the fossil record), as well as higher level entities (e.g., taphonomic groups or pop-
29 ulations). Indeed, at multiple scales and levels of organisation, the spatial patterns ob-
30 served in any palaeontological or archaeological assemblage retain valuable informa-
31 tion about taphonomic accumulation and re-elaboration processes (*sensu* Fernández-
32 López et al., 2002). Spatial taphonomic data, appropriately recorded, can be quantita-
33 tively analysed within a statistical framework in order to reliably draw inferences about
34 taphonomic processes, in turn with consequences for palaeoecological reconstructions
35 (Fernández-Jalvo et al., 2011), biochronological estimates and the interpretation of past
36 human behaviours.

37 In this study, we elaborate on a specific aspect - anisotropy - of the spatial prop-
38 erties of taphonomic entities, with implications for the interpretation of taphonomic
39 processes. Anisotropy, as opposed to isotropy, is generally defined as the property of
40 a process of being directionally dependent. Spatial anisotropic patterns can be seen as
41 products of physical anisotropic processes, such as fluvial or eolian processes, which
42 modified at multiple scales and levels of organisation the original spatial properties of
43 taphonomic entities.

44 At the level of basic taphonomic elements, anisotropy, expressed as preferential
45 orientation of fossils or artefacts, is among the key variables used for interpreting site
46 formation and modification processes. Especially in terrestrial alluvial environments,
47 anisotropy is one of the proxies traditionally used to discriminate autochthonous vs. al-
48 lochthonous assemblages (Petraglia and Nash, 1987; Petraglia and Potts, 1994; Schick,
49 1987; Toots, 1965; Voorhies, 1969, among others). The orientation of elongated ele-
50 ments, prone to preferentially align along the flow direction, would eventually indicate
51 the action of water-flows and suggest substantial transport prior to burial. Nevertheless,
52 anisotropy has been equally documented in autochthonous assemblages subjected to
53 low-energy water-flows (Cobo-Sánchez et al., 2014; Domínguez-Rodrigo et al., 2012,
54 2014d); hence, it can be a necessary but not sufficient condition to differentiate al-
55 lochthony from autochthony (Lenoble and Bertran, 2004). Moreover, besides water-
56 flow processes, anisotropy has been as well observed in association with a wide range
57 of other biostratinomic processes, such as slope processes (Bertran and Texier, 1995)
58 and trampling (Benito-Calvo et al., 2011).

59 Although the anisotropy of basic taphonomic elements have been long studied,
60 the anisotropy of higher level taphonomic entities received by far less attention (see
61 [Markofsky and Bevan, 2012](#) for a directional analysis of archaeological surface distri-
62 butions). Here we address this research gap and conduct a spatial taphonomic study
63 of anisotropy both at the level of fossil specimens and at the assemblage level. The
64 present study uses a comprehensive set of spatial statistics (fabric analysis, geostatis-
65 tics, wavelet analysis, point pattern analysis) in order to identify directional trends that
66 may not be readily apparent. Indeed, beyond the traditional approach of eye-spotting
67 spatial patterns, spatial statistics allow one to adopt a more formal, quantitative ap-
68 proach.

69 Furthermore, at the scale of sedimentary particles, anisotropy is investigated by
70 means of anisotropy of magnetic susceptibility (AMS). AMS refers to the property of
71 elongated magnetic crystals to orient parallel to the flow direction when transported
72 as sedimentary clasts. In sedimentology, AMS analysis is widely applied in order
73 to determine paleoflows in a range of depositional environments, including turbidite
74 systems, contouritic drifts, beaches, deltas and tidal flats ([Felletti et al., 2016](#); [Liu et al.,](#)
75 [2001](#); [Lowrie and Hirt, 1987](#); [Novak et al., 2014](#); [Parés et al., 2007](#), among others).

76 Therefore, integrating the results of our multiscale and multilevel analysis of anisotropy
77 with preliminary remarks about differential taphonomic preservation, sedimentologi-
78 cal and micromorphological observations, we aim to disentangle the taphonomic his-
79 tory of the fossiliferous locality Tsiotra Vryssi (Mygdonia Basin, Macedonia, Greece;
80 [Konidaris et al., 2015](#)).

81 Finally, this study offers an important contribution to the building of a spatial tapho-
82 nomic referential framework for the interpretation of other fossil vertebrate assem-
83 blages, including archaeo-palaeontological ones ([Domínguez-Rodrigo et al., 2017](#)).

84 **2. The palaeontological site of Tsiotra Vryssi (TSR)**

85 Tsiotra Vryssi (TSR) is located in the Mygdonia Basin (Macedonia, Greece), about
86 45 km Southeast of Thessaloniki (Fig. 1). TSR was discovered in 2014 by a joint
87 research team from the Aristotle University of Thessaloniki and the Eberhard Karls

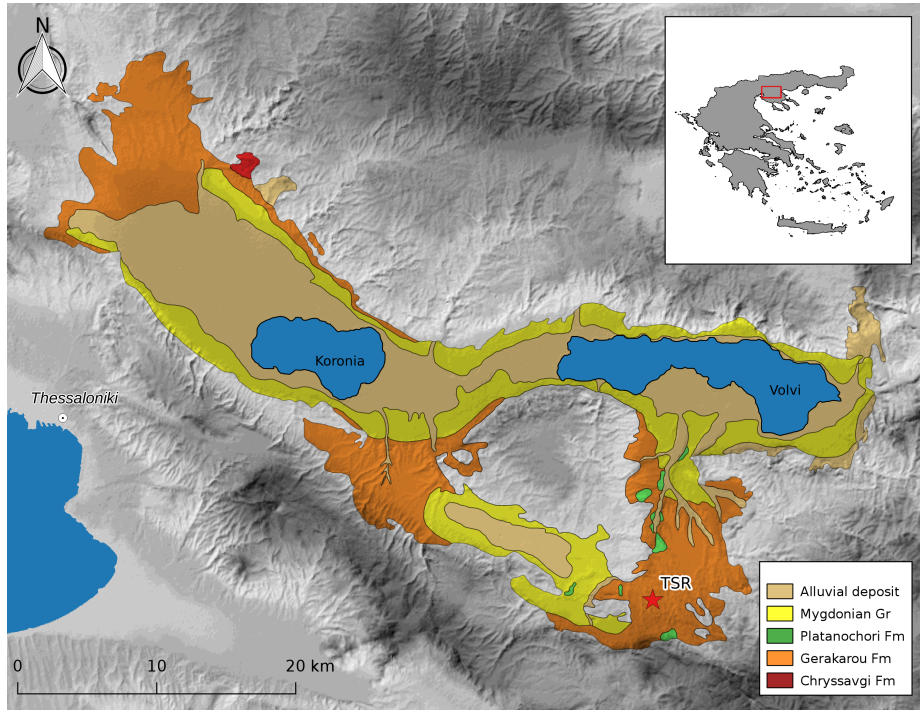


Figure 1: Geological setting of the Mygdonia Basin (Macedonia, Greece) showing the Neogene and Quaternary lithostratigraphic units and the location of Tsiotra Vryssi (TSR), modified after [Koufos et al. \(1995\)](#)

88 University of Tübingen during systematic field surveys in the basin. After the first
 89 collection of fossils from the exposed natural section and the test excavation carried
 90 out in 2014, systematic excavation of the site took place in 2015 and is still ongoing
 91 (Fig. 2a).

92 To date, the excavation covers about a 10 m-thick stratigraphic interval from the
 93 upper Gerakarou Formation (Fig. 1), a suite of continental clastic deposits of mainly
 94 fluvial origin and inter-layered paleosols ([Konidaris et al., 2015; Koufos et al., 1995](#)).
 95 The TSR fauna occurs mainly within a c. 1 m-thick interval of silts (uppermost part
 96 of unit Geo2, see Fig 3) and comprises several mammalian taxa, as well as some birds
 97 and reptiles, whose preliminary biochronological correlation is consistent with a late
 98 Villafranchian (Early Pleistocene) age ([Konidaris et al., 2016, 2015](#)).

99 Two main depositional units are identified (Geo 1 and Geo 2, from younger to older;

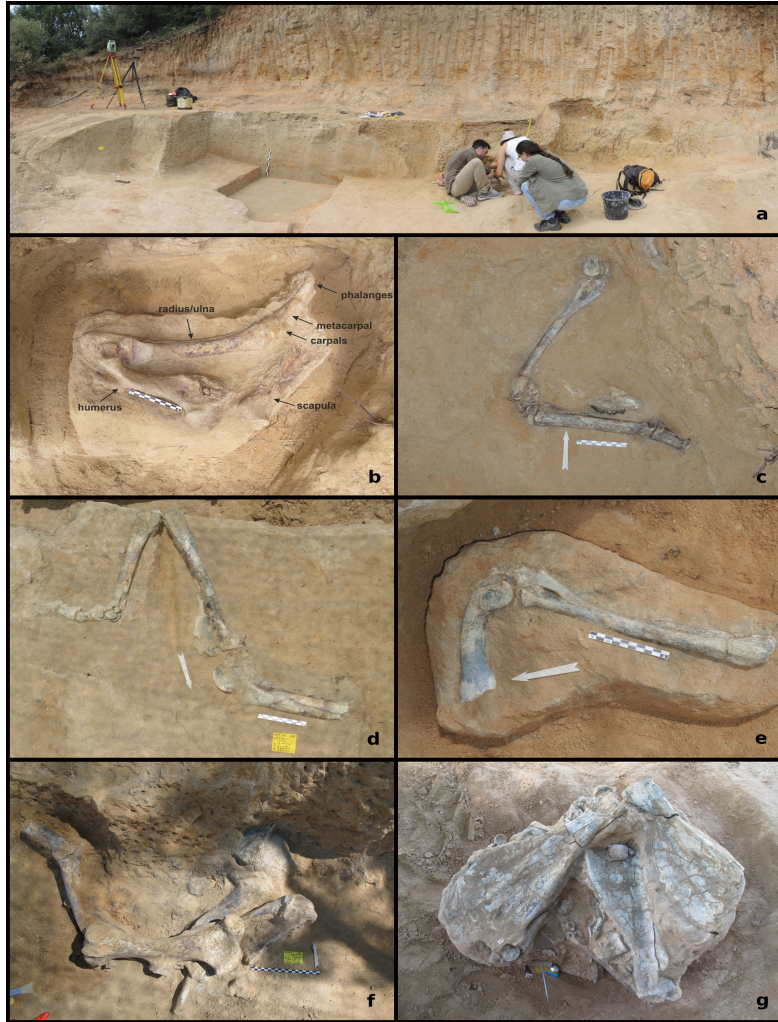


Figure 2: Panoramic view (2017) of the excavation area of Tsiotra Vryssi. Pictures of articulated specimens (a, b, c, d) and clusters of bones (e, f).

100 Fig. 3). The fossiliferous unit Geo 2 begins with ~1.5 m (Geo 2b in Fig. 3) of cross-
101 stratified gravelly sands organised into dm-thick beds with a range of planar to trough-
102 cross laminations. Noteworthy, Geo 2b can be followed laterally for at least 150m in the
103 E-W direction, suggesting an extensive setting of deposition. Above a sharp contact,
104 a few tens of cm of well-sorted, structure-less fine sands follow, which rapidly grade
105 upward into the deposit forming the matrix of the main TSR fossil assemblage (Geo
106 2a in Fig. 3). This is represented by ~1 m of poorly sorted silts (moderately rich in
107 mica grains), locally intercalated by cm-thick lenses of medium-coarse grained sands
108 and relatively more clayey in the uppermost 30 cm of the deposit. Apart for alignment
109 of isolated sand to granule grade clasts and some crude parallel lamination in coarse
110 lenses, the deposits appear overall structure-less. Typically, Geo 2a has a very pale
111 brown colour with a few (less than 10%) pink to reddish yellow mottles, whereas the
112 topmost part of Geo 2a has a strong brown to dark yellowish brown matrix with about
113 the 15-20% of reddish yellow mottles. This change in colour is associated with the
114 occurrence of very small calcareous nodules and common to abundant Mn-Fe-bearing
115 nodules with diameter less than 1 cm (see micromorphological analysis in Section 4.5).

116 Geo 1b is represented by an up to 2 m-thick bed set of cross-stratified gravelly
117 sands and gravels, similar to those observed in Geo 2b (Fig. 3). It sits on top of a basal
118 erosion, down-cutting deeply into older sediments (Geo 2a) and shallowing toward the
119 West. In the same direction, the Geo 1b beds tend to be thinner, finer grained and
120 less extensive laterally, suggesting less energetic hydrodynamic conditions. Though
121 poorly exposed, the younger Geo 1a is represented by a monotonous 3 m-thick section
122 of poorly silty sands devoid of coarse intercalations, which rapidly grades into clayey
123 silts of a distinctive pale brown colour.

124 Overall, the stratigraphic position of TSR in the fluvioterrrestrial Gerakarou Forma-
125 tion ([Koufos et al., 1995](#)) and the specific sedimentary sequence of the site indicate
126 that the TSR assemblage formed in a relatively low energy fluvial environment. A pre-
127 liminary visual inspection of the vertical and horizontal distribution of the fossil finds
128 (Fig. 4) suggests a densely preserved association of fossils (about 24 elements/m²), ho-
129 mogeneously distributed within the study area. Apparent anisotropy is also suggested
130 at assemblage level.

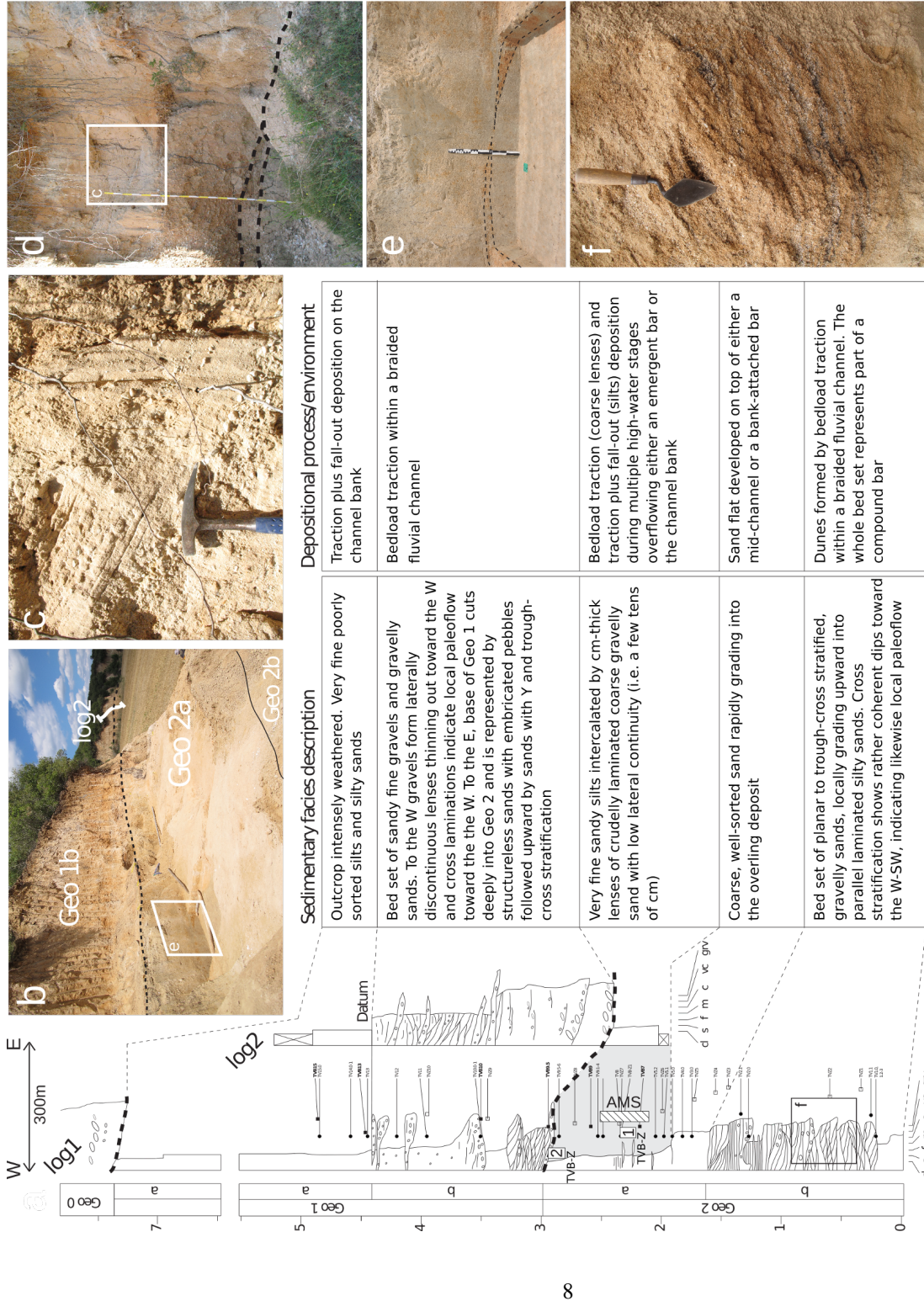


Figure 3: Stratigraphic sedimentary logs (log1 and log 2) with location of main erosional surfaces bounding depositional units Geo 1 and Geo 2, block samples TVB-Z 1 and 2 collected for micromorphology analysis and interval sampled for anisotropy of magnetic susceptibility analysis (AMS); b) WNW-ESE oriented panoramic view of the excavation site and location of the stratigraphic log2 in the background; c) and d) are details of the lower half of log2 showing the basal erosion of Geo 1b followed upward by inclined laminations; e) the middle part of Geo 2a (i.e., the fossiliferous unit) sampled for AMS analysis. Note the presence of cm-thick sand lenses with Fe-hydroxide stains; f) detail of cross stratifications from the top of Geo 2b.

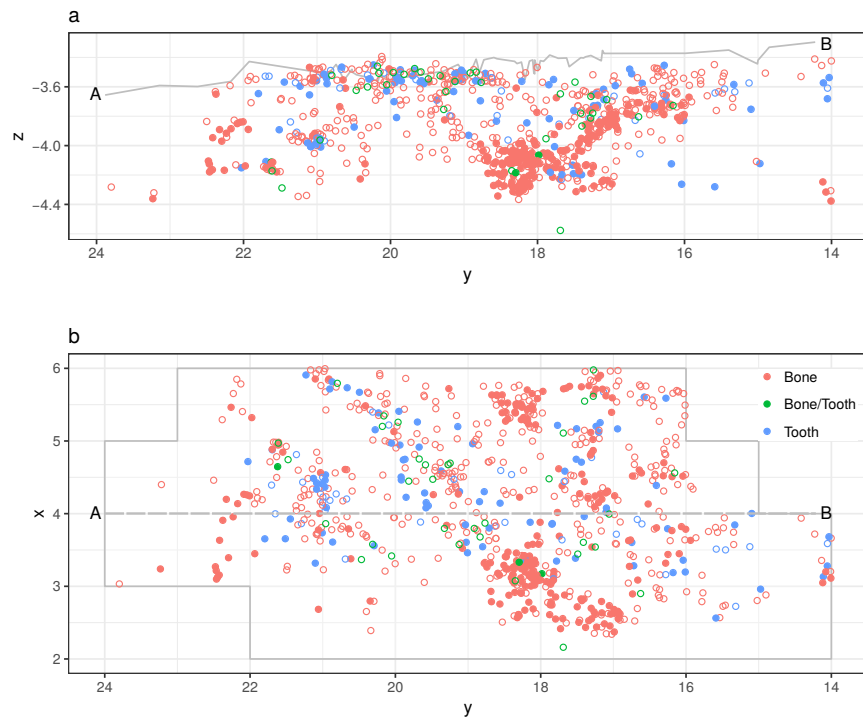


Figure 4: Vertical (a) and horizontal (b) distribution of the sampled fossil specimens from Tsiotra Vryssi (excavations 2015-2017). Filled circles mark complete specimens, hollow circles mark fragmented ones. Grey continuous line in a) marks the Geo 1/2 erosional contact, as recorded at the AB transect marked in b).

131 In such a fluvial depositional context, questions arise with respect to the specific
132 character of the TSR fossil assemblage, the number of depositional events (single or
133 multiple) and the degree of transportation of the fossil record (autochthonous vs. al-
134 lochthonous assemblage).

135 **3. Material and methods**

136 *3.1. Data collection and sub-setting*

137 Since 2015 a grid of 1 m² units was set up and a total station was used in or-
138 der to record the spatial provenience of collected (i.e., diagnostic bones and teeth,
139 and carnivore modified bones) and not collected remains (i.e., non-diagnostic bone
140 fragments with length ≥50 mm; Fig. 2a). Non-diagnostic, or non-carnivore modified
141 bone fragments with length <50 mm were not recorded. This dimensional thresh-
142 old was chosen because small bone fragments show more random orientations than
143 longer specimens (Domínguez-Rodrigo et al., 2014d). Orientation (plunge and bear-
144 ing) of clearly elongated specimens (i.e., specimens with length at least twice the width)
145 was measured with a 1 degree accuracy, using a compass and inclinometer (Eberth
146 et al., 2007; Fiorillo, 1991; Voorhies, 1969, among others). Strike and dip measure-
147 ments were taken along the symmetrical longitudinal a-axis (SLA) of the specimens
148 (Domínguez-Rodrigo and García-Pérez, 2013), using the lowest endpoint of the a-axis
149 as an indicator of the vector direction. The dimensions (length and maximum width)
150 of the recorded finds were measured on-site with a millimetric measuring tape.

151 The present spatial taphonomic study analysed a sample of stratified specimens (n
152 = 797) from the fossiliferous unit Geo 2a, whose spatial coordinates were recorded
153 with the total station. The area of analysis comprises the 34 m² excavated from 2015
154 until 2017. The sample included mostly macromammal remains (n = 707, 89%), unde-
155 termined isolated bone fragments (n = 70), birds (n = 12) and turtle (n = 8) remains. A
156 sub-sample (n = 249) was further subset for the fabric analysis described below. Strat-
157 ified specimens from Geo 2a collected during the test excavation of 2014, or subse-
158 quently found in plaster-jackets with concentration of bones during the lab preparation
159 were excluded due to the lack of precise spatial coordinates. The very small sample (n

= 4) of micromammal remains was also not included in the spatial and faunal analyses.
Faunal analysis was conducted on a sub-sample of complete or fragmented, isolated
or articulated macromammal remains (n = 707). Further sub-setting strategies are de-
scribed below.

As for the AMS analysis, we collected 18 cylindrical oriented samples ($\varnothing = 2.5$
cm) from the middle part of the fossiliferous unit Geo 2a (Fig. 3). AMS analysis was
performed at the Alpine Laboratory of Paleomagnetism in Peveragno (Italy) using a
AGICO KLY-3 Kappabridge susceptibility meter (15-positions, manual oriented).

In order to investigate the micromorphological properties of the Geo 2a unit (i.e.,
sedimentary structures and pedogenetic features), two blocks of undisturbed sediment
were collected from the excavation area; one (TVB-Z 1) from the middle part of the
unit and the other (TVB-Z 2) from the topmost 30 cm of it (Fig. 3). The blocks were
later consolidated for preparation of thin sections following the methods described in
[Murphy \(1986\)](#).

3.2. Spatial anisotropy

Different methods have been developed in neighbouring disciplines to detect spa-
tial anisotropy. Here we use circular statistics for the fabric analysis of taphonomic el-
ements; geostatistics (directional variograms), wavelet analysis and point pattern anal-
ysis for detecting anisotropy at the assemblage level.

3.2.1. Fabric analysis

The first controlled experiments and analyses of the orientation and dispersal of
disarticulated mammal bones as indicators of the depositional context, carried out by
[Toots \(1965\)](#) and [Voorhies \(1969\)](#), led to an increasing number of studies on the effects
of water flows on natural and anthropogenic faunal assemblages ([Aramendi et al., 2017](#);
[Benito-Calvo and de la Torre, 2011](#); [Cobo-Sánchez et al., 2014](#); [de la Torre and Benito-](#)
[Calvo, 2013](#); [Domínguez-Rodrigo et al., 2014a, 2012, 2014d](#); [Fiorillo, 1991](#); [Nash and](#)
[Petruglia, 1987](#); [Organista et al., 2017](#); [Petruglia and Nash, 1987](#); [Petruglia and Potts,](#)
[1994](#); [Schick, 1987](#), among others).

188 Whereas most of these studies have been conducted on disarticulated long bones
189 or elongated bone fragments - which were observed to preferentially align their a-
190 axes along the direction of the flow - relatively few have investigated the hydraulic
191 behaviour of articulated skeletal elements. Flume experiments conducted by [Coard](#)
192 and [Dennell \(1995\)](#) and [Coard \(1999\)](#) demonstrated that articulated bones display a
193 greater transport potential than disarticulated ones when the articulated elements align
194 themselves. However, they also noted that skeletal parts with a higher number of artic-
195 ulated elements, such as complete limbs, may show weak preferential orientation when
196 assuming disorganised spatial configuration, i.e., when not aligned. Therefore, articu-
197 lated bones, although relatively common at TSR (Fig. 2a,b,c,d), were not included in
198 the fabric analysis.

199 In this study we applied circular statistics to a subset of 249 non-articulated, elon-
200 gated bone specimens, having length $\geq 20\text{mm}$ ([Domínguez-Rodrigo et al., 2014d](#)).
201 No distinction of skeletal elements was made, due to the high percentage (91%, n =
202 227) of fragmented remains in the analysed sample - mostly appendicular (n = 122),
203 undetermined (n = 93), axial and cranial (n = 12) fragments - and due to the low per-
204 centage (9%, n = 22) of complete bones - 17 limb bones, 4 scapulae and a rib.

205 We applied Rayleigh and omnibus tests of uniformity, such as Kuiper, Watson and
206 Rao ([Jammalamadaka et al., 2001](#)), to test the isotropic orientation of the fossil speci-
207 mens. Whereas the Rayleigh test assumes a unimodal distribution and assess the sig-
208 nificance of the sample mean resultant length (\bar{R}), the omnibus tests detect multimodal
209 departures from the null hypothesis of circular isotropy.

210 Rose and equal area Schmidt diagrams were used as exploratory data analysis tools
211 to visualise the sample distribution. Compared to the widely used rose diagrams, which
212 plot the circular distribution of the bearing values, the Schmidt equal area diagram
213 informs about the distribution of the three-dimensional orientation (plunge and bearing)
214 of the elements ([Fiorillo, 1988](#)). Points plotting at the margin of the globe indicate
215 planar fabric, whereas points towards the centre have higher dip angles.

216 The Woodcock diagram ([Woodcock and Naylor, 1983](#)), based on three ordered
217 normalised eigenvalues (S_1, S_2, S_3), was used to discriminate between linear (cluster),
218 planar (girdle) and isotropic distributions. In the Woodcock diagram, the C parameter

219 ($C = \ln(S_1/S_3)$) expresses the strength of the preferential orientation, and its signifi-
220 cance is evaluated against critical values from simulated random samples of different
221 sizes. A perfect isotropic distribution would plot at the origin, with equal eigenvalues
222 ($S_1 = S_2 = S_3 = 1/3$). On the other hand, the K parameter ($K = \frac{\ln(S_1/S_2)}{\ln(S_2/S_3)}$) expresses
223 the shape of the distribution, and it ranges from zero (uni-axial girdles) to infinite (uni-
224 axial clusters).

225 In a fluvio-lacustrine environment a cluster distribution would suggest a strong
226 preferential orientation of the sample, such as in the case of channelised water flows
227 (Petraglia and Potts, 1994), whereas a girdle distribution a weaker preferential orienta-
228 tion, spread over a wider range of directions. Overland flows have been interpreted to
229 produce such a pattern (Organista et al., 2017). On the other hand, a isotropic distribu-
230 tion would suggest that post-depositional disturbance by water flows was not strong
231 enough to preferentially orient the assemblage (Domínguez-Rodrigo et al., 2014a).
232 However, a variety of taphonomic processes can produce similar patterns. Fabric anal-
233 ysis, although very informative, has low power by itself. In order to overcome the
234 intrinsic limitations of the fabric analysis, a multivariate approach to site formation and
235 modification processes should be employed (Lenoble and Bertran, 2004).

236 *3.2.2. Geostatistics*

237 Geostatistics refer to a body of concepts and methods typically applied to a limited
238 sample of observations of a continuous variable, for example environmental variables.
239 Geostatistics thus aim to estimate the variance and spatial correlation of known ob-
240 servations and predict, using interpolation methods such as Kriging, unknown values
241 of the variable at non-observed locations. Moreover, by using directional variograms,
242 geostatistics enable the identification of spatial anisotropy (i.e., directional patterns).
243 Since the vast majority of spatial statistics assume stationarity and isotropy, it is well
244 understood that a misinterpretation of spatial anisotropy may result in inaccurate spatial
245 modelling and prediction.

246 Although well known in ecological studies, only a relatively small number of stud-
247 ies have explicitly applied geostatistics to the study of site formation and modifica-
248 tion processes, using directional variograms to investigate the specimens size spa-

tial distributions (Domínguez-Rodrigo et al., 2014a,c), or to specifically detect spatial anisotropy of archaeological assemblages (Bevan and Conolly, 2009; Markofsky and Bevan, 2012).

In order to investigate spatial anisotropy in the distribution of the TSR fossil assemblage and identify spatial continuity in some directions more than others, we used directional variograms and variogram maps. The studied sample includes 797 recorded specimens (isolated or articulated, complete or fragmented bones and teeth) unearthed from Geo 2a and included in the 34 m² window of analysis (Fig. 4). The same sample was used for the wavelet and point pattern analyses.

Specifically, plotting the semi-variance between the variable values of sampled point pairs as a function of distance (spatial lag) between these pairs, directional variograms are used to model the spatial variation at multiple scales and different directions. Three parameters (*nugget*, *range* and *sill*) are estimated from an experimental variogram to fit a theoretical omnidirectional variogram. The *nugget* is used to account for spatial variability at very short distances. The *range* indicates the maximal distance up to which there is spatial correlation. At longer distances the semi-variance levels off forming the *sill*, indicating independence between pairs of sample separated by that minimum distance (Dale and Fortin, 2014; Lloyd and Atkinson, 2004). Thus, we plotted the experimental directional variogram against the theoretical omnidirectional variogram. A directional semi-variance lower than the fitted omnidirectional variogram indicates continuity in the analysed direction. We selected for our analysis the N-S (0°), E-W (90°), NE-SW (45°) and NW-SE (135°) geographical directions. In addition to the directional variograms, variogram maps are visual representations of the semi-variance: the anisotropy is represented by an ellipse, its axes being proportional to the variation expected in each direction. Thus, the direction of maximum anisotropy corresponds with the major axis of the ellipse (Legendre and Legendre, 2012).

3.2.3. Wavelet analysis

As a second method for the detection of spatial anisotropy at the assemblage level we used the wavelet analysis. Wavelet analysis, commonly applied in mathematics for signal processing, has relatively wide application in palaeoclimatology and palaeoecol-

ogy, but is seldom used in studies on site formation processes ([Markofsky and Bevan, 2012](#)).

Unlike the geostatistics approach to the analysis of spatial anisotropy, which is based on a transformation of point values into a continuous surface, the wavelet approach does not apply any transformation, but identifies the elements (points) of a pattern merely by their location. In this regard, the wavelet analysis does not suffer from the arbitrary choice of a surface smooth parameter, as in the case of geostatistics.

For each specific point of the pattern, a wheel of 360 sectors of 1° is used to measure the average variance in the angles between point pairs ([Rosenberg, 2004](#)). The significance of the wavelet analysis is evaluated against 199 Monte Carlo simulations of the observed pattern under the null hypothesis of randomness. The variance is plotted as a function of angle measurements. Direction is measured anti-clockwise from East (i.e., 0° is East, 90° is North). When the distribution of the observed values (dashed line) wanders above the simulated values (continuous line), the pattern shows significant anisotropy in that direction.

[294 3.2.4. Point pattern analysis](#)

A spatial point pattern is the outcome of a random spatial point process. Any natural phenomenon which results in a spatial point pattern, such as a distribution pattern of fossils, can be viewed as a point process ([Baddeley et al., 2015](#)). Therefore, the analysis of a spatial point pattern ultimately addresses the nature of the point process that generated the pattern. Point pattern analysis has been specifically applied to the study of site formation and modification processes by a relatively small number of studies ([Domínguez-Rodrigo et al., 2014a, 2017, 2014c; Giusti and Arzarello, 2016; Giusti et al., in press; Lenoble et al., 2008; Organista et al., 2017](#)). However, this analytical method has never been used to detect anisotropy in the distribution patterns of archaeological or palaeontological assemblages. Nevertheless, detecting anisotropy is an essential part of any spatial analysis. Standard statistical tools in spatial point pattern analysis rely on crucial assumptions about the point process itself: a point process is assumed to be stationary and/or isotropic if its statistical properties are not affected by shifting and/or rotating the point process.

309 In order to further assess the presence of anisotropy in the distribution pattern of the
310 TSR assemblage, we specifically applied the point pair distribution function ($O_{r1,r2}(\Phi)$);
311 [Baddeley et al., 2015](#)). The function estimates the probability distribution of the direc-
312 tions of vectors joining pairs of points that lie more than $r1$ and less than $r2$ units
313 apart. With selected different distances $r1$ and $r2$, the function estimates the multiscale
314 variation of anisotropy. Results are visualised in rose diagrams, where the direction is
315 measured counter-clockwise from East (0°).

316 At the supra-element assemblage level, spatial anisotropy is expected to be detected
317 in a fluvial depositional environment, and most likely to share the same preferential
318 orientation with taphonomic elements. Characteristic elongated lag deposits are typical
319 patterns observed in association with water-flows dragging materials in one direction,
320 the same as the main orientation of the elements ([Domínguez-Rodrigo et al., 2012](#)).

321 *3.3. Anisotropy of magnetic susceptibility (AMS)*

322 The anisotropy of magnetic susceptibility (AMS) is a technique used to identify
323 preferred orientation of magnetic minerals in rocks and unconsolidated sediments ([Hrouda,](#)
324 [1982; Tarling and Hrouda, 1993](#)). It is based on the principle that, when a magnetic
325 field is applied to a sample, the induced magnetisation depends on the bulk orienta-
326 tion of its magnetic constituents. In turn, the AMS magnitude depends on both the
327 anisotropy of individual magnetic particles and the degree of their alignment. Particle
328 anisotropy can be related to either crystalline (anisotropy along a specific crystal plane
329 or axis) or shape (anisotropy along the long axis of the particle) characteristics. Since
330 in most magnetic minerals forming sedimentary particles the long crystallographic axis
331 is the easiest to magnetise (e.g., magnetite), the shape anisotropy is generally dominant,
332 with few exceptions (e.g., haematite).

333 The magnetic susceptibility is represented by three symmetric tensors describing
334 an ellipsoid with three susceptibility axes named K1 to K3 and ordered by decreasing
335 susceptibility. The orientation of the ellipsoid is evaluated projecting the ellipsoid axes
336 on an equal-area projection stereogram. Thus, the shape of the ellipsoid is evaluated
337 using the Flinn or Jelinek scatter plots. In a Flinn (F/L) diagram the foliation along
338 the horizontal axis ($F = K2/K3$; [Stacey et al., 1960](#)) is plotted against the lineation

339 along the vertical axis ($L = K_1/K_2$; [Balsey and Buddington, 1960](#)). Values of $F/L < 1$
 340 indicate oblate ellipsoids (i.e., disc-shaped), whereas values of $F/L > 1$ indicate prolate
 341 ellipsoids (i.e., cigar-shaped) with the axial ratios increasing with distance from the
 342 origin. Alternatively, the AMS magnitude and shape can be visualised on the Jelinek
 343 shape plot ([Jelinek, 1981](#)), by using the corrected anisotropy degree

$$Pj = \exp \sqrt{2[(\ln K_1 - k)^2 + (\ln K_2 - k)^2 + (\ln K_3 - k)^2]}$$

344 where

$$k = \frac{\ln K_1 + \ln K_2 + \ln K_3}{3}$$

345 and the shape parameter

$$T = \frac{\ln L - \ln F}{\ln L + \ln F}$$

346 where samples are prolate for $-1 < T < 0$ or oblate for $0 < T < 1$.

347 In sediments, oblate ellipsoids with imbrication angles less than 20° are considered
 348 diagnostic of primary depositional processes ([Hamilton and Rees, 1970](#); [Hrouda, 1982](#);
 349 [Lanza and Meloni, 2006](#); [Liu et al., 2001](#); [Tarling and Hrouda, 1993](#)). In turn, prolate
 350 ellipsoids mostly relate to post-depositional deformation (e.g., rocks recording tectonic
 351 or metamorphic strain), especially when the magnetic anisotropy is high ([Hrouda and](#)
 352 [Janák, 1976](#)).

353 3.4. Differential preservation

354 Differential preservation, or taphonomic survival, refers to the proportion of tapho-
 355 nomic elements being preserved after the action of environmental factors ([Fernández-](#)
 356 [López, 2006](#)). Selective preservation arises from the differential modification of tapho-
 357 nomic entities, by interaction of inherent properties of the entities with the external
 358 environmental factors. Skeletal elements representation is among the key variables po-
 359 tentially indicative of the selective action of water-flows ([Behrensmeyer, 1975b](#); [Kauf-](#)
 360 [mann et al., 2011](#); [Voorhies, 1969](#), among others). Other variables, not considered

361 in this preliminary study, include breakage patterns, disarticulation patterns and bone
362 surface modifications.

363 The pioneering flume experiments by [Voorhies \(1969\)](#) on disarticulated, complete
364 sheep and coyote bones resulted in a three-group classification of fluvial transport sus-
365 ceptibility of skeletal elements, subsequently elaborated by [Behrensmeyer \(1975b\)](#).
366 Since shape and structural density have been found to influence the transportability of
367 skeletal elements ([Behrensmeyer, 1975b](#); [Boaz, 1982](#)), assemblages subject to moder-
368 ate to high-energy water-flows typically show an under-represented number of smaller,
369 less dense bones. The Voorhies Group I (rib, vertebra, sacrum, sternum) is the most
370 easily affected by fluvial transport; thus its presence or absence in the fossil assemblage
371 informs about the degree of disturbance by water-flows. In turn, the proportion between
372 the represented Voorhies Groups provides evidence for the degree of preservation of the
373 assemblage ([Behrensmeyer, 1975b](#)). We included in the Voorhies groups only com-
374 plete, non-articulated macromammal bones (plus rami of mandibles, and maxillae) of
375 adult individuals - the very few specimens of juvenile individuals, having different hy-
376 draulic behaviour, were excluded. Our grouping criteria followed the classification
377 reported in [Lyman \(1994, Tab.6.5\)](#). Carpals, tarsals and sesamoids were included in
378 Voorhies Group I/II, as the phalanges; maxillae in Group II/III, as the mandibular rami.
379 The studied sample included 147 specimens of Perissodactyla (n = 59), Artiodactyla
380 (n = 41), Carnivora (n = 12) and indeterminate taxa (n = 35). The distribution of deter-
381 minate Voorhies Groups was further categorised in 5 size classes, following the body
382 mass (BM) classification of [Palombo \(2010, 2016\)](#), modified for *Ursus etruscus* after
383 [Koufos et al. \(in press\)](#). The first group (BM1), not present so far in our collection,
384 includes mammals weighing less than 10 kg; BM2 ranges from 10 to 59 kg (*Canis*
385 *etruscus*); BM3 from 60 to 249 kg (*Ursus etruscus*, medium-sized Cervidae); BM4
386 from 250 to 1000 kg (*Equus*, *Bison*, *Praemegaceros*). We excluded from the Voorhies
387 Groups specimens attributed to BM5, that includes very large mammals over 1000 kg
388 weight (Rhinocerotidae and Elephantidae). Nevertheless, their skeletal element rep-
389 resentation was analysed following the Fluvial Transport Index (FTI) classification of
390 [Frison and Todd \(1986\)](#). Undetermined taxa or BM classes - yet in the BM2-BM4
391 range - were also included in the analysis (named NA in Fig. 10).

392 Closely related to the Voorhies Groups, the ratio of complete isolated teeth/vertebrae
393 (T/V) is another indicator of the depositional environment ([Behrensmeyer, 1975b](#)).
394 High-energy fluvial deposits, such as channel-fills and -lag deposits, tend to have high
395 T/V ratio, whereas a low T/V ratio characterises low-energy fluvial deposits, such as
396 that of floodplain deltaic and lacustrine settings ([Lyman, 1994](#)).

397 Complementary to the hydraulic behaviour of complete, isolated faunal remains
398 classified in the Voorhies Groups, the skeletal part representation of fragmented bones
399 provides another indication of the assemblages degree of preservation ([Domínguez-](#)
400 [Rodrigo et al., 2017, 2014d; Pante and Blumenschine, 2010](#)). Vertebrae and ribs, being
401 mostly cancellous, fragile and comparatively less dense, are more susceptible to frag-
402 mentation and transportation, even in low-energy conditions, with respect to cranial
403 and appendicular elements, which are more dense and likely to survive in lag assem-
404 blages ([Domínguez-Rodrigo et al., 2017](#)). In order to integrate the Voorhies Groups,
405 we analysed a sub-sample of 400 isolated macromammal specimens, composed of 315
406 bone and tooth fragments, 78 complete teeth, 1 antler, and 6 appendicular bones of
407 juvenile or BM5 specimens.

408 Finally, the distribution of articulated bones was analysed by anatomical regions. A
409 sub-sample of 50 articulated macromammal units of 154 bone elements were classified
410 as axial (vertebrae, ribs) or appendicular (humeri, femura, radii, tibiae, metapodials,
411 carpal/tarsals and phalanges) units.

412 *3.5. Reproducible research*

413 The subset of the raw data collected for this study, necessary to reproduce the re-
414 ported results, is licensed, except where otherwise specified, under the CC-BY-NC-
415 ND-4.0 license and publicly available at the DOI: [10.5281/zenodo.1435836](https://doi.org/10.5281/zenodo.1435836). The repos-
416 itory includes in addition the code used to process and reduce the data-set. The analy-
417 ses were performed in R: a language and environment for statistical computing ([R Core](#)
418 [Team, 2017](#)); except for the wavelet analysis, performed using the PASSaGE software,
419 version 2 ([Rosenberg and Anderson, 2011](#)). The commented R code needed to repro-
420 duce the reported analyses is released under the MIT license in the same repository.
421 We provide as well a detailed description of the procedure used in PASSaGE.

Table 1: Values and p – *values* of circular uniformity test statistics.

| Sample n | mean dir. | Rayleigh | | Kuiper | | Watson | | Rao | |
|------------|-----------|-----------|-------|--------|-------|--------|-------|----------|--------|
| | | \bar{R} | p | V_n | p | U^2 | p | U | p |
| 249 | 148° | 0.165 | 0.001 | 2.3791 | <0.01 | 0.3957 | <0.01 | 186.5181 | <0.001 |

4. Results

4.1. Anisotropy of basic taphonomic elements

Circular statistics were applied for the fabric analysis of basic taphonomic elements, i.e., isolated, not articulated elongated complete bone specimens or bone fragments. Tab. 1 summarises the results of the circular uniformity tests. The Rayleigh test, which assumes a unimodal distribution, confirmed (p – value = 0.001) the significance of the sample mean resultant length ($\bar{R} = 0.165$). The value of \bar{R} close to 0 indicates that the data are evenly spread around the mean direction ($\bar{\theta} = 148$, SE), with relatively high standard deviation ($\hat{\sigma} = 1.89$) and angular variance ($V = 48$). On the other hand, the Schmidt and rose diagrams (Fig. 5a) showed a multimodal distribution, mostly concentrated in the SE quadrant and with secondary peaks to the N and SW. Accordingly, the Kuiper, Watson and Rao omnibus tests, all rejected the null hypothesis of uniformity at the 99% confidence level, thus suggesting a significant anisotropic multimodal distribution of the fossil sample. Moreover, the Schmidt diagram (Fig. 5a) showed a planar fabric of the sample distribution, with points plotting predominantly on the edge of the equal area hemisphere, thus indicating 0-to-low degree of dip (mean plunge=12°; variance=1.5°).

In the Woodcock diagram (Fig. 5b), the C value (1.89) is higher than the critical S1/S3 test value (1.44) for N=300 at 99% confidence level. Thus, the data sample significantly rejects the hypothesis of randomness in favour of a strong organised sample. The K value (0.11) plots the data sample close to $K = 0$, indicating uniaxial girdles (planar fabric).

4.2. Anisotropy of the taphonomic population

Geostatistics (directional variograms and variogram map), wavelet and point pattern analyses were used for detecting anisotropy at the assemblage level. Fig. 6a shows

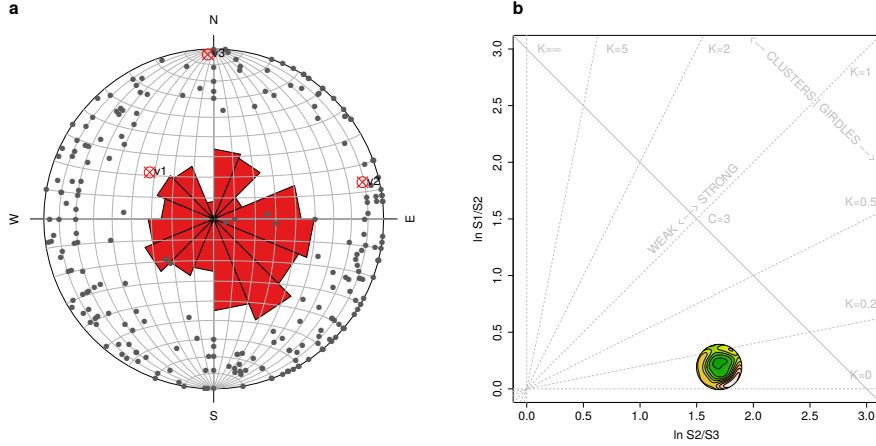


Figure 5: Rose and equal area Schimidt diagrams (a). Woodcock diagram (b).

447 the kernel smooth density estimation ($\sigma = 0.17$) of the sample distribution in the study
 448 area. A preliminary visual examination suggests a NW-SE oriented clustering of the
 449 assemblage, although interfered with secondary NE-SW oriented dispersion. Fig. 6b
 450 shows the variograms in the four main geographical directions (N-S, E-W, NE-SW,
 451 NW-SE), plotted against the omnidirectional fitted variogram. As a rule of thumb, in
 452 order to determine the spatial structure of the sampled data, only the first two-thirds of
 453 the variogram are interpreted (Dale and Fortin, 2014). The omnidirectional variogram
 454 (red line) indicates that at short distance lags, the semi-variances are close to zero,
 455 indicating very strong spatial structure (correlation). With longest distance lags, the
 456 semi-variance rise to a plateau (*sill*) of lack of spatial correlation. The semi-variance
 457 of the NW-SE (135°) direction is lower than in the omnidirectional variogram, start-
 458 ing well before the *sill*, thus indicating continuity (spatial correlation) in that direction.
 459 Minor directional trends are also detected in the N-S (0°), and to a lesser extent in the
 460 NE-SW (45°) directions. This result is clearly confirmed by the diagonal striping in the
 461 variogram map (Fig. 6c). The map shows a major ellipse oriented NW-SE, with minor
 462 parallel structures.

463 As for the wavelet analysis, Fig. 7 plots the variance as function of the direction,
 464 ranging anti-clockwise from 0° (E) to 180° (W). A major peak is evident at 135° (NW),

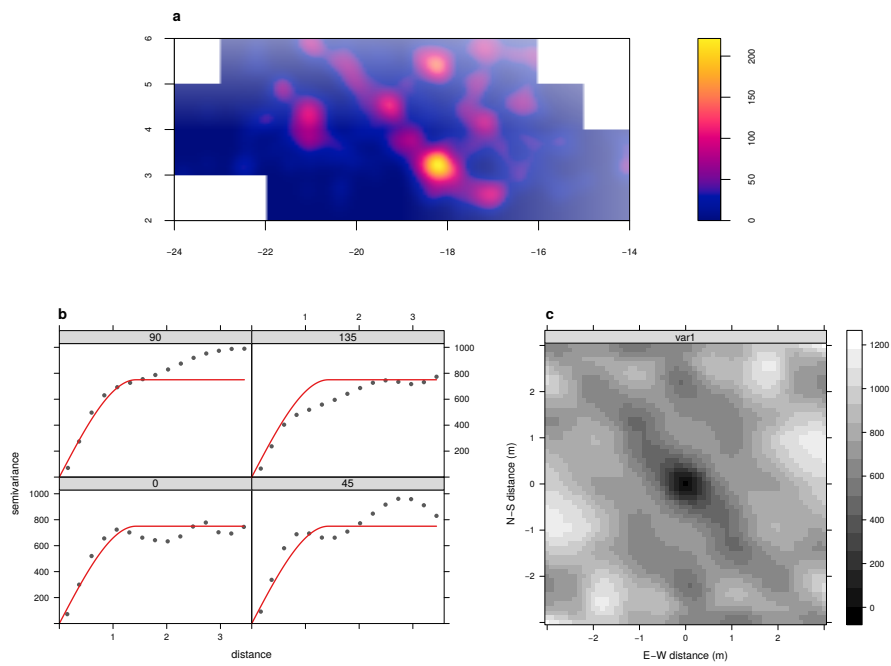


Figure 6: Kernel smoothed intensity function of the fossil assemblage (a). Directional variograms (4 clockwise directions from N-S, 0°) shown as grey points alongside the fitted omnidirectional variogram shown as a continuous red line (b) and variogram map (c).

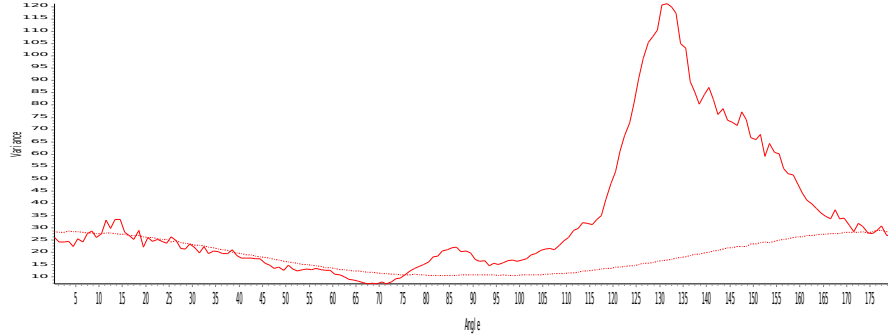


Figure 7: Angular wavelet graph. Angles range from 0° (E) to 180° (W). Peaks of variance (continuous line) indicate the direction of maximum anisotropy. Dashed line marks the Monte Carlo simulated null hypothesis of isotropy.

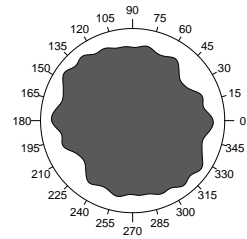
wandering way above the expected values for a random (isotropic) pattern. A secondary significant peaks, although of much less intensity, is present at 85° (N). In accordance with the directional variograms, the wavelet analysis indicates a significant anisotropy in the NW-SE direction. Moreover, it suggests minor occurrence of points (specimens) in the N-S direction, as also indicated by the geostatistics analysis. However, in contrast with the directional variograms, the angular wavelet graph does not support significant preferential orientation in the NE range (angles between 0° and 90°).

Fig. 8 shows the results of our point pattern analysis and specifically the point pair distribution function $O_{r1,r2}(\Phi)$ for a range of distances $r1 = 0.01$ m and $0.25 < r2 < 1.5$ m. The plot illustrates the multiscale variation of anisotropy, from a uniform, isotropic pattern (for $r2 = 0.25$ m), to increased anisotropy in the NW-SE direction. The maximum anisotropy is observed for $r2 = 1$ m, as elements at a maximum distance of 1 m show the strongest directional pattern. With increased distances of $r2 > 1$ m, the rose diagrams suggest the addition of a second orthogonal NE-SW directional trend, which reflects the parallel alternation of NW-SE bands in the assemblage distribution.

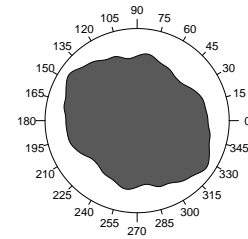
4.3. Anisotropy of magnetic susceptibility

In Fig. 9a, the AMS of the whole sample set ($n = 18$) is investigated. The equal-area projection of the three susceptibility axes K1-K3 (left-hand side of Fig. 9a) in-

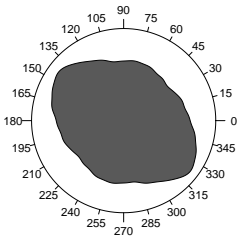
r=0.25



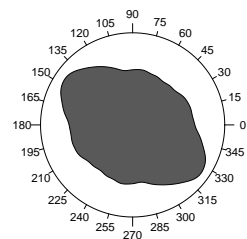
r=0.5



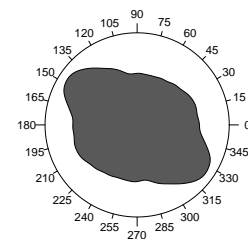
r=0.75



r=1



r=1.25



r=1.5

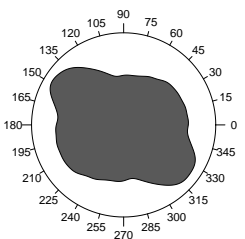


Figure 8: Rose diagrams of the point pair distribution function for a range of distances ($0.25 < r_2 < 1.5$ m). Direction is measured counter-clockwise from East (0°).

484 dicates high variability of the axes orientation, with confidence angles of the K1 and
485 K2 mean directions largely overlapping. This result suggests no preferential orienta-
486 tion of the axes. However, the Flinn and Jelinek plots (right-hand side of Fig. 9a)
487 reveal the presence of 7 samples with prolate ellipsoids, thus suggesting the action of
488 post-depositional deformation processes which could have obliterated the primary de-
489 positional pattern. Therefore, in order to overcome possible post-depositional noise,
490 further AMS analysis focused only on a sub-set of samples showing oblate ellipsoids
491 ($n = 11$). In Fig. 9b, the equal-area projection shows a well defined clustering of the
492 axes, with the maximum anisotropy axis K1 aligned along the NW-SE direction and the
493 K3 imbrication angles varying within a wide range of angles (from 4° to 85°). Because
494 high K3 imbrication angles may result from post-depositional rehash of sediments, fur-
495 ther analysis were conducted on a selection of 5 samples with K3 imbrication angles
496 less than 20° (Hamilton and Rees, 1970; Hrouda, 1982; Lanza and Meloni, 2006; Liu
497 et al., 2001; Tarling and Hrouda, 1993). In Fig. 9c, the equal-area projection indicates
498 again a NW-SE orientation of the maximum anisotropy axis K1. Despite the small
499 sample size, the AMS analysis suggests a weak anisotropy of magnetic sedimentary
500 grains along a NW-SE direction.

501 *4.4. Differential preservation*

502 Fig. 10a shows the distribution at the family level of the whole sampled material.
503 Determined taxa included Perissodactyla, Artiodactyla, Carnivora and Proboscidea,
504 together with a number of undetermined bone fragments (44%). The histogram shows
505 the prominent presence of Equidae over other taxa (27%), followed by Bovidae (11%)
506 and Cervidae (5%). However, it is worth noting the presence of very large mammals
507 (body mass class BM5), such as Elephantidae and the rhinocerotid *Stephanorhinus* sp.,
508 and to a less extent, of carnivores, such as *Canis etruscus* and *Ursus etruscus*.

509 The distribution of the Voorhies Groups plotted by body mass classes is shown
510 in Fig. 10b. BM1 is so far not present in the TSR assemblage, while BM2 includes
511 the *C. etruscus*, BM3 includes the medium-sized Cervidae and *Ursus etruscus*, BM4
512 the medium- and large-sized *Equus* sp., *Bison* sp. and the large-sized cervid *Prae-*
513 *megaceros* sp. Notably, the Voorhies Group III is represented in Fig. 10b only by the

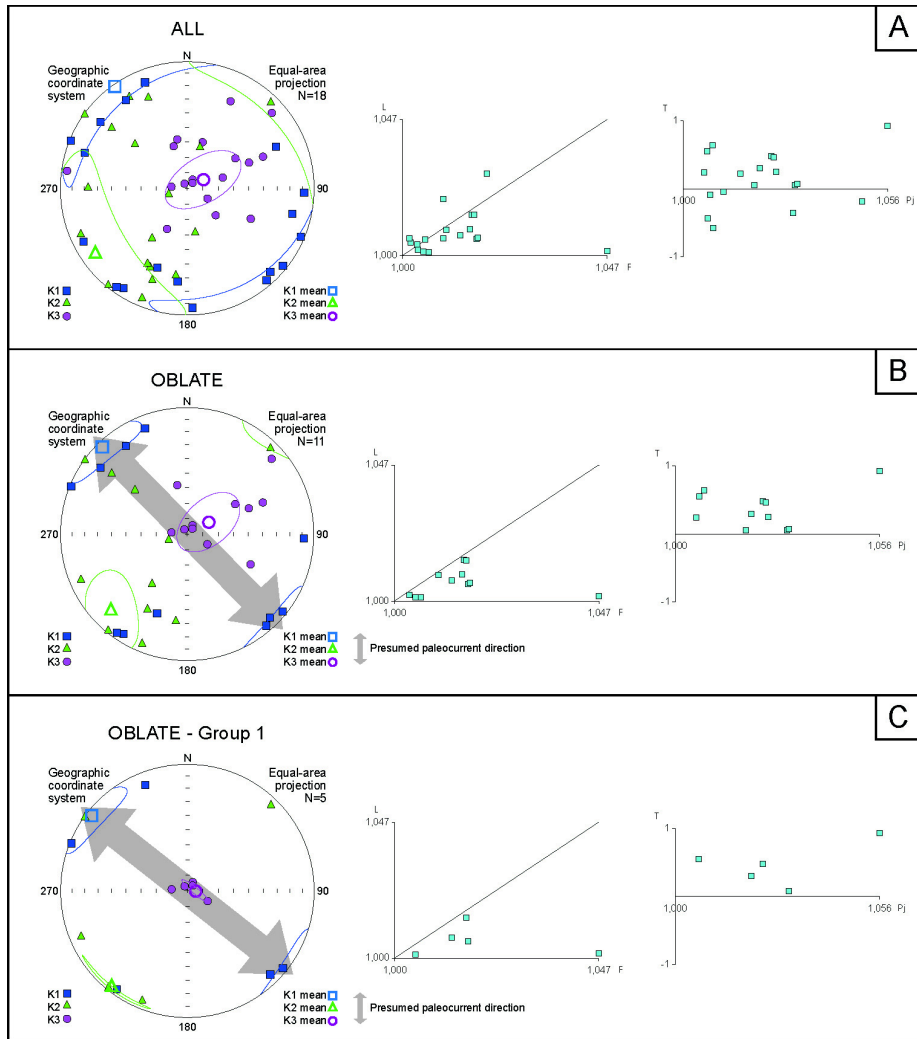


Figure 9: Equal-area projection stereogram (left-hand side) of the anisotropy axes K1, K2 and K3 (with $K_1 > K_2 > K_3$) and Flinn and Jelinek plots (right-hand side) for a) all the samples; b) samples with oblate-shaped anisotropy ellipsoid; c) samples with K_3 imbrication angle less than $20-25^\circ$.

514 crania of the carnivores *Canis* and *Ursus*. Moreover, the fossil record of *U. etruscus* in
515 included maxilla fragments (Voorhies Group II/III), isolated teeth, 2 articulated vertebrae
516 and an ulna fragment. Specimens from the BM4 grouped mostly in II/III, II, I/II and
517 showed lack of Voorhies Group I and III. On the other hand, the bulk of undetermined
518 BM specimens plotted in Voorhies Group I/II, with some occurrence in Group I, II, and
519 to a less extent in Group II/III.

520 Fig. 10c shows the side-by-side distribution of complete and fragmented isolated
521 macromammal skeletal elements. Firstly, the skeletal element distribution of complete
522 specimens suggests a very high teeth/vertebra ratio (7.8). The ratio (3) is lower, but
523 still relatively high when considering isolated, fragmented specimens. Limb bone and
524 undetermined fragments represent the majority of the fragmented, isolated specimens,
525 as compared to axial skeletal parts.

526 Accordingly, the prominent presence of appendicular skeletal elements over axial
527 is also showed in the distribution of articulated specimens (Fig. 10d), which account
528 for 22% of the sampled assemblage. Articulated lower limb elements (metapodes,
529 carpals/tarsals, phalanges) represent the majority of bones, often articulated to frag-
530 mented upper elements (radii, tibiae, humeri, femora). Interestingly, some of the latter
531 elements present carnivore gnawing marks (Fig. 2e).

532 4.5. Micromorphology

533 The TVB-Z 1 block (Fig. 3) consists mostly of poorly sorted sandy silts, composi-
534 tionally dominated by metamorphic quartz and accessory metamorphic minerals. From
535 bottom to top, several sharp grain size breaks occur, which partition the sampled inter-
536 val into mm-thick normally graded laminae, displaying an upward increase of matrix
537 content (Fig. 11a). This includes clay infilling pore spaces (Fig. 11a) and suggests
538 either flow velocity fluctuations or multiple waning depositional events. Birefringent
539 illuvial clay coatings are also present along some voids (Fig. 11b), thus indicating in-
540 cipient pedogenesis, likely due to temporary subaerial exposure (Kühn et al., 2010).

541 Most of the thickness of the TVB-Z 2 block (Fig. 3) displays similar characteris-
542 tics to the TVB-Z 1 block, except for the presence of rolled soil clasts (pedorelicts;
543 Fig. 11c), likely eroded from nearby locations (Cremaschi et al., In press). Conversely,

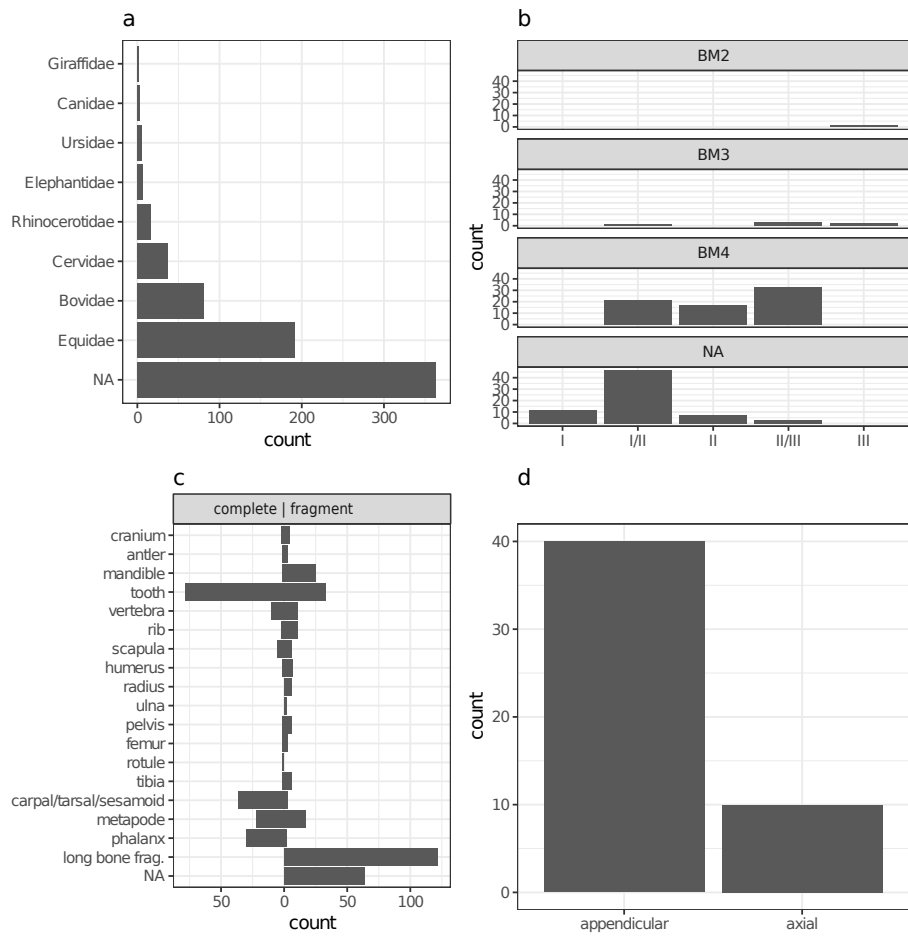


Figure 10: Distribution at the family level of the whole sampled material (a). Voorhies Groups distribution of the complete, isolated macromammal bones (plus rami of mandibles and maxillae) by body mass (BM) (b). Side-by-side distribution of complete/fragmented isolated macromammal skeletal elements (c). Skeletal region distribution of articulated macromammal specimens (d).

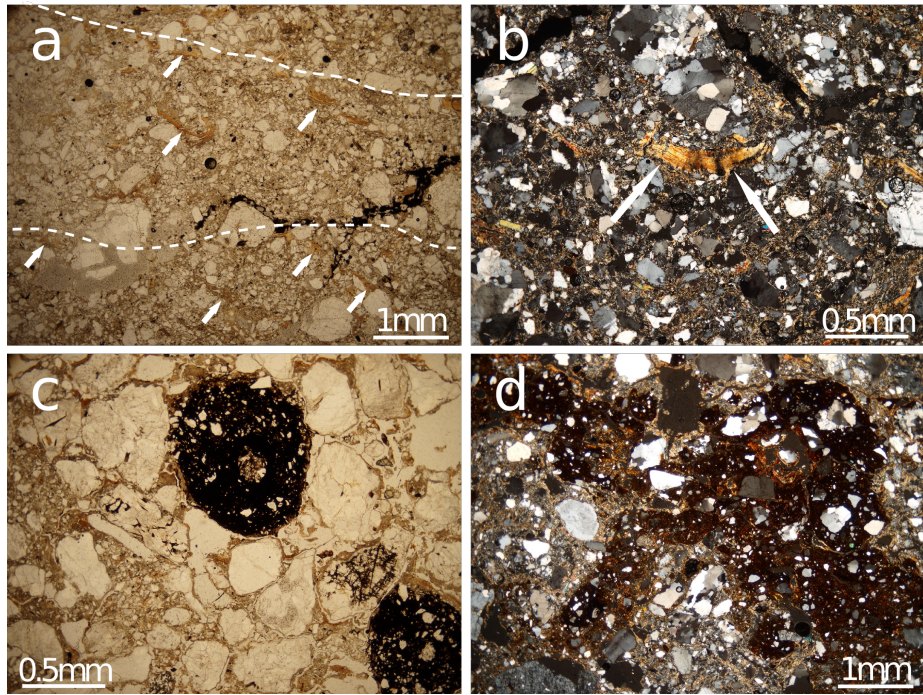


Figure 11: Microphotographs showing a) clast alignments (dashed white lines), crude normal grading and clays infilling pore spaces (arrows) from block TVB-Z 1 in parallel polarised light (PPL); b) illuvial clay coating a planar void from sample TVB-Z 1 in cross polarised light (XPL); c) rolled pedorelict (a Fe/Mn nodule developed on quartz grain) from topmost part of block TVB-Z 2 (PPL); d) Fe oxide hypocoatings on the groundmass and illuvial clay coating of voids from topmost part of block TVB-Z 2 (XPL).

544 the uppermost part of the sample (Fig. 11d) displays moderate clay illuviation along
 545 sparse voids most likely related to bioturbation and impregnating redoximor-
 546 phic features (Lindbo et al., 2010). The latter include Fe oxide hypocoatings on the
 547 groundmass, Fe/Mn oxide nodules with regular outline developed on quartz grains,
 548 and fragmented clay coatings. Altogether, these features suggest that, after deposi-
 549 tion, Geo 2a underwent moderate pedogenesis due to a relatively prolonged phase of
 550 subaerial exposure in a warm and possibly humid climate or while still saturated with
 551 water.

552 **5. Discussion**

553 Spatial taphonomy has recently emerged as a new methodological framework com-
554 plement to the traditional taphonomic approach (Domínguez-Rodrigo et al., 2017). By
555 using spatial statistical methods, spatial taphonomy aims to investigate the multiscale
556 and multilevel spatial properties of different taphonomic entities (*sensu* Fernández-
557 López, 2006). Indeed, taphonomic alteration processes work simultaneously, at dif-
558 ferent scales, on entities of different level of organisation, from the basic taphonomic
559 elements (bone specimens), to higher level taphonomic groups (taphons) or popula-
560 tions (assemblages). For example, dispersion processes of taphonomic elements may
561 modify their spatial location, orientation and removal degree. At the same time, disper-
562 sion of taphonomic elements may also cause changes in the density, spatial distribution
563 and representatives of elements of each taphon or taphonic population (Fernández-
564 López, 2006). Thus, beside the traditional taphonomic approach, the results of spatial
565 taphonomy are of great importance for investigating the natural or cultural processes
566 of dispersal and accumulation of faunal or cultural remains, in turn with consequences
567 for palaeoecological reconstructions, biochronological estimates and past human be-
568 havioural inferences.

569 In this regard, this study offers an initial contribution to the development of a so far
570 non-existent referential framework for the spatial taphonomic interpretation of palaeon-
571 tological or archaeological assemblages (Domínguez-Rodrigo et al., 2017). Indeed,
572 the taphonomic study of non-human related bone assemblages has great importance
573 for archaeological research as well. As an example, water-flow processes are recog-
574 nised to be among the most important natural processes in the formation and modifi-
575 cation of a significant percentage of the vertebrate fossil and archaeological sites alike
576 (Behrensmeyer, 1975a, 1982, 1988; Coard, 1999; Coard and Dennell, 1995; Petraglia
577 and Nash, 1987; Petraglia and Potts, 1994; Schiffer, 1987; Voorhies, 1969, among
578 others). Under the effect of water-flows, assemblages may adopt a variety of forms,
579 ranging from (peri)autochthonous rearranged assemblages and biased lag assemblages
580 to transported, allochthonous assemblages (Behrensmeyer, 1988; Domínguez-Rodrigo
581 and García-Pérez, 2013). One fundamental assumption behind reliable inferences on

582 past human behaviour is the pristine preservation of the depositional context. There-
583 fore, it is essential, in order to fully comprehend the archaeological record, to test
584 within a referential framework alternative taphonomic hypotheses.

585 In this study, taphonomic dispersion and accumulation processes were analysed
586 focusing on a specific aspect - anisotropy - of the spatial properties of taphonomic enti-
587 ties. A multilevel analysis of anisotropy was conducted at the level of basic taphonomic
588 elements and at the assemblage level. Anisotropy, defined as the preferential orienta-
589 tion of skeletal elements, constitutes a fundamental part of any taphonomic study (Ara-
590 mendí et al., 2017; Benito-Calvo and de la Torre, 2011; Cobo-Sánchez et al., 2014;
591 de la Torre and Benito-Calvo, 2013; Domínguez-Rodrigo et al., 2014a, 2012, 2014d;
592 Fiorillo, 1991; Nash and Petraglia, 1987; Organista et al., 2017; Petraglia and Nash,
593 1987; Petraglia and Potts, 1994; Schick, 1987; Toots, 1965; Voorhies, 1969, among
594 others). However, spatial anisotropy at supra-element level of taphons or assemblages
595 is an often neglected taphonomic criterion that should be reconsidered, especially in
596 spatial taphonomic analyses of fluvial dispersion and accumulation processes. Never-
597 theless, standard spatial statistics rely on crucial assumptions about the isotropy of the
598 spatial processes responsible for the observed spatial pattern (Baddeley et al., 2015).

599 We investigated the multilevel spatial anisotropy and selective composition of the
600 fossiliferous deposit of Tsiotra Vryssi, from the fluvial Gerakarou Formation of the
601 Mygdonia Basin, Greece. Specific research questions regarded the character and num-
602 ber of depositional processes and the degree of re-elaboration of the fossil record. Spe-
603 cific aspects of our results are discussed below.

604 5.1. Recursive anisotropy

605 Recursive anisotropy emerged at the level of basic taphonomic elements and at the
606 assemblage level. Fabric analysis, geostatistics, wavelet and point pattern analyses all
607 pointed to a preferential NW-SE orientation of the assemblage and the sub-sample of
608 elongated bone specimens.

609 Fabric analysis, or the analysis of the orientation (plunge and bearing) of elongated
610 elements, can provide valuable insight into taphonomic processes, allowing discrimi-
611 nation between different orientation patterns (isotropic, linear or planar). We analysed

612 a sub-sample of not articulated, clearly elongated bone specimens, mostly limb bone
613 fragments. Articulated units were excluded from the fabric analysis since experimental
614 studies by [Coard and Dennell \(1995\)](#) and [Coard \(1999\)](#) reported that articulated units
615 with a higher number of elements, such as complete limbs, may show weak preferen-
616 tial orientation when not aligned, as they often occur at TSR (Fig. 2c,d,e). Otherwise,
617 the authors concluded that articulated bones showed a greater than expected hydraulic
618 transport potential. Thus, their conspicuous presence in the TSR fossil record (about
619 22%) would not necessarily suggest an autochthonous deposit.

620 The results of the circular uniformity test statistics (Tab. 1) agreed upon rejecting
621 the null hypothesis of uniformity, suggesting a significant anisotropic distribution of the
622 fossil sample. The Schimdt and Woodcock diagrams in Fig. 5 indicated planar fabric
623 (0-to-low degree of dip) and a girdle pattern, with preferential orientation towards the
624 SE. In girdle distribution elements orient over a wider sector of angles than cluster dis-
625 tributions, yet showing higher anisotropy than random distributions. Whereas cluster,
626 linear patterns are associated with channelised water-flows ([Petruglia and Potts, 1994](#)),
627 girdle, planar patterns have been interpreted as products of overland flows (runoff;
628 [Organista et al., 2017](#)). The preferential orientation of the sampled elongated bones
629 suggests that the TSR fossil deposit most likely underwent relatively high-energy, but
630 non-channelised NW-SE water-flows. However, anisotropy does not itself discriminate
631 between allochthonous and autochthonous deposits. Autochthonous lag assemblages
632 undergoing minimal re-sedimentation could also exhibit significant anisotropic spatial
633 patterns ([Domínguez-Rodrigo et al., 2012, 2014b, 2017, 2014c](#)). Since a wide range of
634 different taphonomic processes can produce similar patterns, an unequivocal discrim-
635 ination based only on fabric observations is seldom possible, and other taphonomic
636 criteria should be considered ([Lenoble and Bertran, 2004](#)).

637 Geostatistics, wavelet and point pattern analyses were applied in order to detect
638 anisotropy of the TSR fossil assemblage. All these different methods agreed on iden-
639 tifying a preferentially NW-SE oriented distribution. Four directional variograms and
640 a variogram map (Fig. 6b,c) were calculated from a kernel density estimation of the
641 assemblage spatial distribution (Fig. 6a). Small, dense clusters of fossils, although
642 occurring at different elevations in the 1m-thick vertical distribution (Fig. 4a), con-

643 catenate along a prevailing NW-SE direction. Secondary minor directions (N-S and
644 NE-SW) were identified in the directional variograms (Fig. 6b). In the same manner,
645 the wavelet graph (Fig. 7) and the rose diagrams (Fig. 8) also detected a strong pref-
646 erential NW-SE directional distribution. Similar elongated lag deposits are typically
647 associated with water-flows dragging material in one direction ([Domínguez-Rodrigo](#)
648 [et al., 2012](#)).

649 These observations are in agreement with the AMS results. Despite the small sam-
650 ple size, the AMS results suggest relatively strong anisotropy, with a mean K1 axis
651 oriented NW-SE and a mean K2 axis oriented NE-SW, although with much smaller
652 confidence angles (Fig. 9). Since K1 (i.e., the axis of maximum anisotropy) should
653 reflect the bulk orientation of the elongated axis of the ferro/paramagnetic sedimentary
654 particles, it might be concluded that AMS hints at a NW-SE oriented anisotropy.

655 Thus, the observed recursive multilevel anisotropy patterns most probably points
656 to the action of NW-SE oriented water-flows, at the specific location of the TSR site.
657 However, both analyses of isotropy at element level (fabric analysis) and assemblage
658 level (geostatistics, wavelet and point pattern analyses) suggested some degree of noise
659 in the prevalent NW-SE distributions toward other directions, especially to the or-
660 thogonal NE-SW direction. Whereas long bones can roll orthogonally to the main
661 direction of the flow ([Voorhies, 1969](#)), noise in the main directional trend at assem-
662 blage level may indicate multiple depositional processes, or secondary reworking post-
663 depositional processes. Moreover, the relatively high average density of preserved ele-
664 ments ($24/m^2$) occur in small, well defined clusters (Figs. 2f,e, 4 and 6a). Such spatial
665 aggregation of taphonomic elements may be the result of a combination or the sum of
666 different taphonomic processes ([Fernández-López et al., 2002](#)). On the other hand, the
667 formation of gaps in the spatial distribution and clusters of elements in correspondence
668 with topographic depression may as well be associated with lag deposits ([Petricchia and](#)
669 [Potts, 1994](#)). This is likely to happen on top of rippled surfaces or small dunes in the
670 channel-belt. However, there is no evidence of such structure at TSR.

671 5.2. Differential preservation

672 According to the evolutionary and systemic theory of taphonomy, taphonomic al-
673 teration is not only conceived as a destructive process, but it also has positive effects
674 with the preservation and creation of new taphonomic groups. In this sense, the dif-
675 ferential destruction (or taphonomic sieve) of taphonomic entities is just a particular
676 case of taphonomic alteration, as it is the differential modification that gives rise to
677 selective preservation ([Fernández-López, 2006](#)). Intrinsic and extrinsic taphonomic
678 factors determine the differential preservation of taphonomic entities. In this study we
679 integrated our spatial taphonomic approach with a preliminary study of the differential
680 preservation of fossil elements.

681 In the BM4 class of mammals, the relatively high abundance of skeletal elements
682 belonging to the Voorhies Groups I/II, II and II/III (Fig. [10b](#)) suggests minor winnow-
683 ing of the assemblage, with preservation of the densest elements that are above the
684 threshold of transportability ([Behrensmeyer, 1988](#)). Indeed, skeletal elements in the
685 Voorhies Group I (ribs, vertebrae, sacrum, sternum) tend to be transported more easily
686 by saltation or flotation in relatively low-energy currents ([Voorhies, 1969](#)). The under-
687 representation of the Voorhies Group III (crania and complete mandibles) in the BM4
688 class is balanced by the high occurrence of cranial elements in the Group II/III (rami
689 of mandibles and maxilla fragments). Thus, the distribution in Fig. [10b](#) suggests, more
690 than the taphonomic sieve of the Voorhies Group III, a higher fragmentation rate of
691 cranial elements in the BM4 class of mammals (*Equus*, *Bison*, *Praemegaceros*). On
692 the other hand, the Voorhies Group III is better represented in the BM classes 2 and
693 3, which include smaller mammals, i.e., *C. etruscus*, *U. etruscus* and medium-sized
694 cervids. The presence of better preserved carnivore cranial elements, as well as the
695 presence of a partial articulated skeleton of a wolf-sized carnivore, would suggest an
696 autochthonous or para-autochthonous assemblage ([Behrensmeyer, 1988](#)).

697 Although excluded from the Voorhies Group analysis, it is worth noting the pres-
698 ence of several mostly complete skeletal elements of Elephantidae (e.g., ribs, scapula,
699 humerus and several articulated carpals, metacarpals and phalanges) with different FTI
700 values, comparable to elements of the Voorhies Group II and III ([Frison and Todd,](#)
701 [1986](#)). Their distribution suggests that the assemblage was winnowed of the elements

702 with highest FTI, which are comparable to elements of the Voorhies Group I. This is
703 also the case for the other excluded megaherbivore, the rhinocerotid *Stephanorhinus*,
704 which is represented by several teeth and limb bones.

705 Overall, the very high teeth/vertebra ratio (7.8) also supports the hypothesis of a lag,
706 winnowed assemblage. Moreover, the actual presence of a high number of limb and
707 undetermined bone fragments, together with complete appendicular and axial elements
708 (Fig. 10c) supports also some degree of sorting (taphonomic sieve) of the smallest,
709 cancellous fragments. Segregation of axial elements from epiphyses and shafts has
710 been observed even in low-energy fluvial environments (Domínguez-Rodrigo et al.,
711 2017).

712 On the other hand, as noted earlier, the conspicuous presence of articulated spec-
713 imens in the TSR fossil assemblage does not necessarily suggest an autochthonous
714 deposition, since articulated bones may as well show a great hydraulic transport po-
715 tential (Coard, 1999; Coard and Dennell, 1995). Nevertheless, it is worth noting that
716 the distribution of articulated units at TSR shows a significant presence of appendicu-
717 lar elements over axial ones (Fig. 10d). Thus, the under-representation of articulated
718 axial elements also indicates a winnowed, lag assemblage formed by the densest and
719 most resilient elements, with sieve and transport of part of the lighter and more can-
720 cellous elements. However, carnivore ravaging alike tends to eliminate or at least lead
721 to under-representation of those skeletal elements (the less dense, axial elements) in
722 the transport group most prone to be transported by water (Domínguez-Rodrigo et al.,
723 2012; Voorhies, 1969). Interestingly, a preliminary analysis of the bone breakage pat-
724 terns suggests that carnivores had some active role in the modification and possibly in
725 the accumulation of bones at TSR (Fig. 2e; Konidaris et al., 2015).

726 In conclusion, considering the results of our spatial taphonomic analysis, pro-
727 cesses of taphonomic dispersion, such as fluvial accumulation processes, would have
728 likely separated and disseminated the most cancellous taphonomic elements, favouring
729 the persistence of taphons constituted by allochthonous elements (Fernández-López,
730 2006). Carnivores could have likely been primary accumulation agents. However, the
731 recursive anisotropic spatial patterns, at the level of taphonomic elements and at the
732 assemblage level, as well as the clustering pattern in relatively small, dense, aggre-

gations of elements aligned in parallel NW-SE oriented bands, suggest that the TSR deposit resulted from multiple taphonomic dispersion events, with winnowing of less dense, lighter elements and spatial anisotropic re-arrangement of a lag, autochthonous assemblage accumulated over the migrating banks of a NW-SE oriented fluvial system. As suggested by [Organista et al. \(2017\)](#), it is likely for secondary over-bank flows to aggregate bones dispersed over the bank surface into topographic depressions, where they accumulate and acquire greater stability.

Noteworthy, both Geo 1 and Geo 2 show fining upward trends and facies sequences similar to those typical of braided rivers ([Miall, 1977](#)). In such a sequence, the lower coarser-grained part would represent one or more sets of sinuous-crested medium-scale bedforms (i.e., small dunes) forming by bedload traction in the deeper reaches of channels, whereas the upper muddy part is dominantly deposited by decantation either on top of in-channel or bank-attached emerging bars or in floodplains, occasionally provided with coarse material at high-water stages ([Miall, 1982](#)). Therefore, the excavated section can be viewed as the product of cyclical lateral switching of a braided fluvial system.

6. Conclusions

Spatial taphonomy is the systemic, multiscale and multilevel study of the spatial properties of taphonomic processes. Indeed, taphonomic alteration processes work simultaneously, at different scales, on entities of different levels of organisation, from the basic taphonomic elements (bone specimens), to higher level taphonomic groups (taphons) or populations (assemblages). In this study we elaborated on a specific aspect - anisotropy - of the spatial properties of taphonomic processes, investigating an often neglected aspect of the spatial distribution of taphonomic populations.

A multilevel analysis of anisotropy was conducted for the Early Pleistocene fossiliferous locality Tsiotra Vryssi, from the fluvial Gerakarou Formation of the Mygdonia Basin, Greece. Differential preservation of skeletal elements was also analysed in order to unravel the character and number of depositional processes and the degree of re-elaboration of the TSR fossil record. The results of the analyses suggested repeated

762 taphonomic dispersion processes, with winnowing of less dense, lighter elements and
763 spatial anisotropic re-arrangement of a lag, autochthonous assemblage possibly accu-
764 mulated over the migrating banks of a NW-SE oriented fluvial system.

765 We believe that this study contributes towards the development of a referential
766 framework for the spatial taphonomic interpretation of other palaeontological, as well
767 as archaeological, localities.

768 **Acknowledgements**

769 This research was supported by the European Research Council [ERC StG PaGE
770 'Paleoanthropology at the Gates of Europe: Human evolution in the southern Balkans'
771 283503, 2014] and [ERC CoG CROSSROADS 'Human Evolution at the Crossroads'
772 724703, 2017] awarded to K. Harvati. We are grateful to all the participants in the
773 survey and excavation campaigns that took place in the Mygdonia Basin for their in-
774 dispensable contribution.

775 **References**

- 776 Aramendi, J., Uribelarrea, D., Arriaza, M. C., Arráiz, H., Barboni, D., Yravedra, J.,
777 Ortega, M. C., Gidna, A., Mabulla, A., Baquedano, E., Domínguez-Rodrigo, M.,
778 2017. The paleoecology and taphonomy of AMK (Bed I, Olduvai Gorge) and its
779 contributions to the understanding of the "Zinj" paleolandscape. Palaeogeography,
780 Palaeoclimatology, Palaeoecology 488, 35–49.
781 URL [http://www.sciencedirect.com/science/article/pii/
782 S0031018216308112](http://www.sciencedirect.com/science/article/pii/S0031018216308112)
783 Baddeley, A., Rubak, E., Turner, R., 2015. Spatial Point Patterns: Methodology and
784 Applications with R. Chapman and Hall/CRC, London.
785 URL <http://www.crcpress.com/books/details/9781482210200/>
786 Balsey, J. R., Buddington, A. F., 1960. Magnetic susceptibility anisotropy and fabric
787 of some adirondack granites and orthogneisses. American Journal of Science 258,
788 6–20.

- 789 Behrensmeyer, A., 1975a. Taphonomy and paleoecology in the hominid fossil record.
790 Yearbook of Physical Anthropology 19, 36–50.
- 791 Behrensmeyer, A. K., 1975b. The taphonomy and paleoecology of Plio-Pleistocene
792 vertebrate assemblages East of Lake Rudolf, Kenya. Bulletin of the Museum of
793 Comparative Zoology 146, 473–578.
- 794 Behrensmeyer, A. K., 1982. Time resolution in fluvial vertebrate assemblages. Paleobi-
795 ology 8 (3), 211–227.
- 796 Behrensmeyer, A. K., 1988. Vertebrate preservation in fluvial channels. Palaeogeogra-
797 phy, Palaeoclimatology, Palaeoecology 63 (1), 183–199.
- 798 URL <http://www.sciencedirect.com/science/article/pii/003101828890096X>
- 799
- 800 Benito-Calvo, A., de la Torre, I., 2011. Analysis of orientation patterns in Olduvai
801 Bed I assemblages using GIS techniques: Implications for site formation processes.
802 Journal of Human Evolution 61 (1), 50–60.
- 803 URL <http://www.sciencedirect.com/science/article/pii/S0047248411000649>
- 804
- 805 Benito-Calvo, A., Martínez-Moreno, J., Mora, R., Roy, M., Roda, X., 2011. Trampling
806 experiments at Cova Gran de Santa Linya, Pre-Pyrenees, Spain: their relevance for
807 archaeological fabrics of the Upper–Middle Paleolithic assemblages . Journal of
808 Archaeological Science 38 (12), 3652–3661.
- 809 URL <http://www.sciencedirect.com/science/article/pii/S0305440311003153>
- 810
- 811 Bertran, P., Texier, J.-P., 1995. Fabric Analysis: Application to Paleolithic Sites.
812 Journal of Archaeological Science 22 (4), 521–535.
- 813 URL <http://www.sciencedirect.com/science/article/pii/S0305440385700507>
- 814
- 815 Bevan, A., Conolly, J., 2009. Modelling spatial heterogeneity and nonstationarity in
816 artifact-rich landscapes. Journal of Archaeological Science 36 (4), 956–964.

- 817 URL [http://www.sciencedirect.com/science/article/pii/
S0305440308002653](http://www.sciencedirect.com/science/article/pii/S0305440308002653)
- 819 Boaz, D. D., 1982. Modern riverine taphonomy: its relevance to the interpretation of
820 Plio-Pleistocene hominid paleoecology in the Omo basin, Ethiopia. Ph.D. thesis.
- 821 Boaz, N. T., Behrensmeyer, A. K., 1976. Hominid taphonomy: Transport of human
822 skeletal parts in an artificial fluvial environment. American Journal of Physical
823 Anthropology 45 (1), 53–60.
- 824 URL <http://dx.doi.org/10.1002/ajpa.1330450107>
- 825 Coard, R., 1999. One bone, two bones, wet bones, dry bones: Transport potentials
826 under experimental conditions. Journal of Archaeological Science 26 (11), 1369–
827 1375.
- 828 URL [http://www.sciencedirect.com/science/article/pii/
S0305440399904387](http://www.sciencedirect.com/science/article/pii/S0305440399904387)
- 830 Coard, R., Dennell, R., 1995. Taphonomy of some articulated skeletal remains:
831 Transport potential in an artificial environment. Journal of Archaeological Science
832 22 (3), 441–448.
- 833 URL [http://www.sciencedirect.com/science/article/pii/
S030544038570043X](http://www.sciencedirect.com/science/article/pii/S030544038570043X)
- 835 Cobo-Sánchez, L., Aramendi, J., Domínguez-Rodrigo, M., 2014. Orientation patterns
836 of wildebeest bones on the lake Masek floodplain (Serengeti, Tanzania) and their
837 relevance to interpret anisotropy in the Olduvai lacustrine floodplain. Quaternary
838 International 322–323 (0), 277–284, the Evolution of Hominin Behavior during the
839 Oldowan-Acheulian Transition: Recent Evidence from Olduvai Gorge and Peninj
840 (Tanzania).
- 841 URL [http://www.sciencedirect.com/science/article/pii/
S1040618213005363](http://www.sciencedirect.com/science/article/pii/S1040618213005363)
- 843 Cremaschi, M., Trombino, L., Zerboni, A., In press. Palaeosoils and relict soils, a
844 systematic review. In: Stoops, G., Marcelino, V., Mees, F. (Eds.), Interpretation

- 845 of micromorphological features of soils and regoliths – Revised Edition. Elsevier,
846 Oxford, pp. 873–904.
- 847 Dale, M., Fortin, M., 2014. Spatial Analysis: A Guide for Ecologists, second edition
848 Edition. Cambridge University Press.
- 849 de la Torre, I., Benito-Calvo, A., 2013. Application of GIS methods to retrieve
850 orientation patterns from imagery; a case study from Beds I and II, Olduvai Gorge
851 (Tanzania). Journal of Archaeological Science 40 (5), 2446–2457.
- 852 URL [http://www.sciencedirect.com/science/article/pii/
853 S0305440313000113](http://www.sciencedirect.com/science/article/pii/S0305440313000113)
- 854 Domínguez-Rodrigo, M., Bunn, H., Mabulla, A., Baquedano, E., Uribelarrea,
855 Pérez-González, A., Gidna, A., Yravedra, J., Diez-Martin, F., Egeland, C.,
856 Barba, R., Arriaza, M., Organista, E., Ansón, M., 2014a. On meat eating and
857 human evolution: A taphonomic analysis of BK4b (Upper Bed II, Olduvai Gorge,
858 Tanzania), and its bearing on hominin megafaunal consumption . Quaternary
859 International 322–323, 129–152, the Evolution of Hominin Behavior during the
860 Oldowan-Acheulian Transition: Recent Evidence from Olduvai Gorge and Peninj
861 (Tanzania).
- 862 URL [http://www.sciencedirect.com/science/article/pii/
863 S1040618213006198](http://www.sciencedirect.com/science/article/pii/S1040618213006198)
- 864 Domínguez-Rodrigo, M., Bunn, H., Pickering, T., Mabulla, A., Musiba, C., Baque-
865 dano, E., Ashley, G., Diez-Martin, F., Santonja, M., Uribelarrea, D., Barba, R.,
866 Yravedra, J., Barboni, D., Arriaza, C., Gidna, A., 2012. Autochthony and orientation
867 patterns in Olduvai Bed I: a re-examination of the status of post-depositional biasing
868 of archaeological assemblages from FLK North (FLKN). Journal of Archaeological
869 Science 39 (7), 2116–2127.
- 870 URL [http://www.sciencedirect.com/science/article/pii/
871 S030544031200091X](http://www.sciencedirect.com/science/article/pii/S030544031200091X)
- 872 Domínguez-Rodrigo, M., Bunn, H. T., Yravedra, J., 2014b. A critical re-evaluation of
873 bone surface modification models for inferring fossil hominin and carnivore inter-

- 874 actions through a multivariate approach: Application to the FLK Zinj archaeofaunal
875 assemblage (Olduvai Gorge, Tanzania). Quaternary International 322–323 (0), 32–
876 43, the Evolution of Hominin Behavior during the Oldowan-Acheulian Transition:
877 Recent Evidence from Olduvai Gorge and Peninj (Tanzania).
- 878 URL [http://www.sciencedirect.com/science/article/pii/
879 S104061821300760X](http://www.sciencedirect.com/science/article/pii/S104061821300760X)
- 880 Domínguez-Rodrigo, M., Cobo-Sánchez, L., Yravedra, J., Uribelarrea, D., Arriaza, C.,
881 Organista, E., Baquedano, E., 2017. Fluvial spatial taphonomy: a new method for the
882 study of post-depositional processes. Archaeological and Anthropological Sciences,
883 1–21.
- 884 URL <http://dx.doi.org/10.1007/s12520-017-0497-2>
- 885 Domínguez-Rodrigo, M., Diez-Martín, F., Yravedra, J., Barba, R., Mabulla, A.,
886 Baquedano, E., Uribelarrea, D., Sánchez, P., Eren, M. I., 2014c. Study of the
887 SHK Main Site faunal assemblage, Olduvai Gorge, Tanzania: Implications for Bed
888 II taphonomy, paleoecology, and hominin utilization of megafauna. Quaternary
889 International 322–323, 153–166.
- 890 URL [http://www.sciencedirect.com/science/article/pii/
891 S104061821300743X](http://www.sciencedirect.com/science/article/pii/S104061821300743X)
- 892 Domínguez-Rodrigo, M., Fernández-López, S., Alcalá, L., 2011. How Can Taphon-
893 omy Be Defined in the XXI Century? Journal of Taphonomy 9 (1), 1–13.
- 894 Domínguez-Rodrigo, M., García-Pérez, A., 07 2013. Testing the Accuracy of Different
895 A-Axis Types for Measuring the Orientation of Bones in the Archaeological and
896 Paleontological Record. PLoS ONE 8 (7), e68955.
- 897 URL <http://dx.doi.org/10.1371%2Fjournal.pone.0068955>
- 898 Domínguez-Rodrigo, M., Uribelarrea, D., Santonja, M., Bunn, H., García-Pérez,
899 Pérez-González, A., Panera, J., Rubio-Jara, S., Mabulla, A., Baquedano, E.,
900 Yravedra, J., Diez-Martín, F., 2014d. Autochthonous anisotropy of archaeological
901 materials by the action of water: experimental and archaeological reassessment
902 of the orientation patterns at the Olduvai sites. Journal of Archaeological Science

- 903 41 (0), 44–68.
- 904 URL [http://www.sciencedirect.com/science/article/pii/
S0305440313002756](http://www.sciencedirect.com/science/article/pii/S0305440313002756)
- 906 Eberth, D. A., Rogers, R. R., Fiorillo, A. R., 2007. A practical approach to the study of
907 bonebeds. In: Rogers, R. R., Eberth, D. A., Fiorillo, A. R. (Eds.), Bonebeds. Genesis,
908 Analysis, and Paleobiological Significance. The University of Chicago Press, pp.
909 265–332.
- 910 Efremov, I. A., 1940. Taphonomy: a new branch of paleontology. Pan American
911 Geologist 74, 81–93.
- 912 URL [http://www.academia.dk/BiologiskAntropologi/Tafonomi/
Efremov_1940.php](http://www.academia.dk/BiologiskAntropologi/Tafonomi/Efremov_1940.php)
- 914 Felletti, F., Dall’Olio, E., Muttoni, G., 2016. Determining flow directions in turbidites:
915 An integrates sedimentological and magnetic fabric study of the Miocene Marnoso
916 Arenacea Formation (northern Apennines, Italy). Sedimentary Geology 335, 197–
917 215.
- 918 Fernández-Jalvo, Y., Scott, L., Andrews, P., 2011. Taphonomy in palaeoecological
919 interpretations. Quaternary Science Reviews 30 (11), 1296–1302.
- 920 URL [http://www.sciencedirect.com/science/article/pii/
S0277379110002842](http://www.sciencedirect.com/science/article/pii/S0277379110002842)
- 922 Fernández-López, R. S., Fernández-Jalvo, Y., Alcalá, L., 2002. Accumulation: taphonomic
923 concept and other palaeontological uses. In: Renzi, M. D., Alonso, M. P.,
924 Belinchón, M., Peñalver, E., Montoya, P., Márquez-Aliaga, A. (Eds.), Current Top-
925 ics on Taphonomy and Fossilization. pp. 37–47.
- 926 Fernández-López, S., 2006. Taphonomic alteration and evolutionary taphonomy. Journal
927 of Taphonomy 4 (3), 111–142.
- 928 Fiorillo, A. R., 1988. A proposal for graphic presentation of orientation data from
929 fossils. Contributions to Geology 26 (1), 1–4.

- 930 Fiorillo, A. R., 1991. Taphonomy and depositional setting of Careless Creek Quarry
931 (Judith River Formation), Wheatland County, Montana, U.S.A. *Palaeogeography,*
932 *Palaeoclimatology, Palaeoecology* 81 (3), 281–311.
- 933 URL <http://www.sciencedirect.com/science/article/pii/003101829190151G>
- 935 Frison, G. C., Todd, L. C., 1986. *The Colby Mammoth Site: Taphonomy and Archae-*
936 *ology of a Clovis Kill in Northern Wyoming.* University of New Mexico Press.
- 937 Giusti, D., Arzarello, M., 2016. The need for a taphonomic perspective in spatial
938 analysis: Formation processes at the Early Pleistocene site of Pirro Nord (P13),
939 Apricena, Italy. *Journal of Archaeological Science: Reports* 8, 235–249.
- 940 URL <http://www.sciencedirect.com/science/article/pii/S2352409X16302656>
- 942 Giusti, D., Tourloukis, V., Konidaris, G., Thompson, N., Karkanas, P., Panagopoulou,
943 E., Harvati, K., in press. Beyond maps: Patterns of formation processes at the
944 Middle Pleistocene open-air site of Marathousa 1, Megalopolis basin, Greece.
945 *Quaternary International.*
- 946 URL <https://www.sciencedirect.com/science/article/pii/S1040618217309795>
- 948 Hamilton, N., Rees, A. J., 1970. The use of magnetic fabric in palaeocurrent estimation.
949 In: Runcorn, S. K. (Ed.), *Palaeogeophysics.* Academic, London, pp. 445–464.
- 950 Hill, A., 1976. On carnivore and weathering damage to bone. *Current Anthropology*
951 17, 335–336.
- 952 Hrouda, F., 1982. Magnetic anisotropy of rocks and its application in geology and
953 geophysics. *Geophysical Surveys* 5 (1), 37–82.
- 954 Hrouda, F., Janák, F., 1976. The changes in shape of the magnetic susceptibility ellip-
955 soid during progressive metamorphism and deformation. *Tectonophysics* 34, 135–
956 148.

- 957 Jammalamadaka, S., Sengupta, A., Sengupta, A., 2001. Topics in Circular Statistics.
958 Series on multivariate analysis. World Scientific.
- 959 URL <https://books.google.de/books?id=sKqWMGqQXQkC>
- 960 Jelinek, V., 1981. Characterization of the magnetic fabrics of rocks. Tectonophysics 79,
961 63–67.
- 962 Kaufmann, C., Gutiérrez, M. A., Álvarez, M. C., González, M. E., Massigoge, A.,
963 2011. Fluvial dispersal potential of guanaco bones (*Lama guanicoe*) under con-
964 trolled experimental conditions: the influence of age classes to the hydrodynamic
965 behavior. Journal of Archaeological Science 38 (2), 334–344.
- 966 URL <http://www.sciencedirect.com/science/article/pii/S0305440310003201>
- 967 Konidaris, G. E., Kostopoulos, D. S., Koufos, G. D., V., T., Harvati, K., 2016. Tsio-
968 tra Vryssi: a new vertebrate locality from the Early Pleistocene of Mygdonia Basin
969 (Macedonia, Greece). In: XIV Annual Meeting of the European Association of Ver-
970 tebrate Palaeontologists. Koninklijke Nederlandse Akademie Van Wetenschappen,
971 p. 37.
- 972 Konidaris, G. E., Tourloukis, V., Kostopoulos, D. S., Thompson, N., Giusti, D.,
973 Michailidis, D., Koufos, G. D., Harvati, K., 2015. Two new vertebrate localities
974 from the Early Pleistocene of Mygdonia Basin (Macedonia, Greece): Preliminary
975 results. Comptes Rendus Palevol 14 (5), 353–362.
- 976 URL <http://www.sciencedirect.com/science/article/pii/S1631068315000706>
- 977 Koufos, G. D., Konidaris, G. E., Harvati, K., in press. Revisiting *Ursus etruscus*
978 (Carnivora, Mammalia) from the Early Pleistocene of Greece with description of
979 new material. Quaternary International.
- 980 URL <http://www.sciencedirect.com/science/article/pii/S1040618217306985>
- 981 Koufos, G. D., Syrides, G. E., Kostopoulos, D. S., Koliadimou, K. K., 1995. Pre-
982 liminary results about the stratigraphy and the palaeoenvironment of Mygdonia
- 983

- 986 Basin, Macedonia, Greece. *Geobios* 28 (Supplement 1), 243–249, first European
987 Palaeontological Congress.
- 988 URL [http://www.sciencedirect.com/science/article/pii/
989 S0016699595801715](http://www.sciencedirect.com/science/article/pii/S0016699595801715)
- 990 Kühn, P., Aguilar, J., Miedema, R., 2010. Textural pedofeatures and related horizons.
991 In: Stoops, G., Marcelino, V., Mees, F. (Eds.), *Interpretation of micromorphological*
992 *features of soils and regoliths*. Elsevier, Oxford, pp. 217–250.
- 993 Lanza, R., Meloni, A., 2006. *The Earth's Magnetism: An Introduction to Geologists*.
994 Springer, Berlin.
- 995 Legendre, P., Legendre, L., 2012. *Numerical Ecology. Developments in Environmental*
996 *Modelling*. Elsevier Science.
- 997 Lenoble, A., Bertran, P., 2004. Fabric of Palaeolithic levels: methods and implications
998 for site formation processes. *Journal of Archaeological Science* 31 (4), 457 – 469.
999 URL [http://www.sciencedirect.com/science/article/pii/
1000 S0305440303001432](http://www.sciencedirect.com/science/article/pii/S0305440303001432)
- 1001 Lenoble, A., Bertran, P., Lacrampe, F., 2008. Solifluction-induced modifications
1002 of archaeological levels: simulation based on experimental data from a modern
1003 periglacial slope and application to French Palaeolithic sites. *Journal of Archaeo-*
1004 *logical Science* 35 (1), 99 – 110.
1005 URL [http://www.sciencedirect.com/science/article/pii/
1006 S0305440307000489](http://www.sciencedirect.com/science/article/pii/S0305440307000489)
- 1007 Lindbo, D. L., Stolt, M. H., Vepraskas, M. J., 2010. Redoximorphic features. In:
1008 Stoops, G., Marcelino, V., Mees, F. (Eds.), *Interpretation of micromorphological*
1009 *features of soils and regoliths*. Elsevier, Oxford, pp. 129–147.
- 1010 Liu, B., Saito, Y., Yamazaki, T., Abdelayem, A., Oda, H., Hori, K., Zhao, Q., 2001.
1011 Paleocurrent analysis for the Late Pleistocene-Holocene incised-valley fill of the
1012 Yangtze delta, China by using anisotropy of magnetic susceptibility data. *Marine*
1013 *Geology* 176, 175–189.

- 1014 Lloyd, C., Atkinson, P., 2004. Archaeology and geostatistics. *Journal of Archaeological Science* 31 (2), 151 – 165.
- 1015
- 1016 URL <http://www.sciencedirect.com/science/article/pii/S0305440303001067>
- 1017
- 1018 Lowrie, W., Hirt, A. M., 1987. Anisotropy of magnetic susceptibility in the scaglia
1019 rossa pelagic limestone. *Earth and Planetary Science Letters* 82, 349–356.
- 1020 Lyman, R., 1994. Vertebrate Taphonomy. Cambridge Manuals in Archaeology. Cam-
1021 bridge University Press.
- 1022 Lyman, R. L., 2010. What taphonomy is, what it isn't, and why taphonomists should
1023 care about the difference. *Journal of Taphonomy* 8 (1), 1–16.
- 1024 Markofsky, S., Bevan, A., 2012. Directional analysis of surface artefact distributions:
1025 a case study from the Murghab Delta, Turkmenistan. *Journal of Archaeological
1026 Science* 39 (2), 428 – 439.
- 1027 URL <http://www.sciencedirect.com/science/article/pii/S030544031100358X>
- 1028
- 1029 Miall, A. D., 1977. Lithofacies Types and Vertical Profile Models in Braided River
1030 Deposits: A Summary. In: Miall, A. D. (Ed.), *Fluvial Sedimentology*. Vol. Memoir
1031 5. Canadian Society of Petroleum Geologists, Calgary, pp. 597–604.
- 1032 Miall, A. D., 1982. Analysis of fluvial depositional systems. AAPG, Tulsa, Okla.
- 1033 Murphy, C. P., 1986. Thin section preparation of soils and sediments. AB Academic
1034 Publishers, Berkhamsted.
- 1035 Nash, D. T., Petraglia, M. D. (Eds.), 1987. Natural formation processes and the archae-
1036 ological record. Vol. 352 of International Series. British Archaeological Reports,
1037 Oxford.
- 1038 Novak, B., Housen, B., Kitamura, Y., Kanamatsuc, T., Kawamura, K., 2014. Magnetic
1039 fabric analyses as a method for determining sediment transport and deposition in
1040 deep sea sediments. *Marine Geology* 356, 19–30.

- 1041 Organista, E., Domínguez-Rodrigo, M., Yravedra, J., Uribelarrea, D., Arriaza, M. C.,
1042 Ortega, M. C., Mabulla, A., Gidna, A., Baquedano, E., 2017. Biotic and abiotic
1043 processes affecting the formation of {BK} Level 4c (Bed II, Olduvai Gorge) and
1044 their bearing on hominin behavior at the site. *Palaeogeography, Palaeoclimatology,*
1045 *Palaeoecology* 488, 59–75.
- 1046 URL [http://www.sciencedirect.com/science/article/pii/
1047 S0031018216306800](http://www.sciencedirect.com/science/article/pii/S0031018216306800)
- 1048 Palombo, M. R., 2010. A scenario of human dispersal in the northwestern Mediterranean throughout the Early to Middle Pleistocene. *Quaternary International* 223–224 (0), 179–194.
- 1049 URL [http://www.sciencedirect.com/science/article/pii/
1050 S1040618209004145](http://www.sciencedirect.com/science/article/pii/S1040618209004145)
- 1051 Palombo, M. R., 2016. To what extent could functional diversity be a useful tool in
1052 inferring ecosystem responses to past climate changes? *Quaternary International*
1053 413 (Part B), 15–31.
- 1054 URL [http://www.sciencedirect.com/science/article/pii/
1055 S1040618215007806](http://www.sciencedirect.com/science/article/pii/S1040618215007806)
- 1056 Pante, M. C., Blumenschine, R. J., 2010. Fluvial transport of bovid long bones
1057 fragmented by the feeding activities of hominins and carnivores. *Journal of Archaeological Science* 37 (4), 846 – 854.
- 1058 URL [http://www.sciencedirect.com/science/article/pii/
1059 S0305440309004324](http://www.sciencedirect.com/science/article/pii/S0305440309004324)
- 1060 Parés, J. M., Hassold, N. J. C., Rea, D. K., van der Pluijm, B. A., 2007. Paleocurrent directions from paleomagnetic reorientation of magnetic fabrics in deep-sea sediments
1061 at the Antarctic Peninsula Pacific margin (ODP sites 1095, 1101). *Marine Geology*
1062 242, 261–269.
- 1063 Petraglia, M. D., Nash, D. T., 1987. The impact of fluvial processes on experimental sites. In: Nash, D. T., Petraglia, M. D. (Eds.), *Natural formation processes and*

- 1069 the archaeological record. Vol. 352 of International Series. British Archaeological
1070 Reports, Oxford, pp. 108–130.
- 1071 Petraglia, M. D., Potts, R., 1994. Water Flow and the Formation of Early Pleistocene
1072 Artifact Sites in Olduvai Gorge, Tanzania. *Journal of Anthropological Archaeology*
1073 13 (3), 228–254.
- 1074 URL [http://www.sciencedirect.com/science/article/pii/
1075 S0278416584710142](http://www.sciencedirect.com/science/article/pii/S0278416584710142)
- 1076 R Core Team, 2017. R: A Language and Environment for Statistical Computing. R
1077 Foundation for Statistical Computing, Vienna, Austria.
1078 URL <https://www.R-project.org/>
- 1079 Rosenberg, M., Anderson, C., 2011. Passage: Pattern analysis, spatial statistics and
1080 geographic exegesis. version 2. *Methods in Ecology and Evolution* 2 (3), 229–232.
- 1081 Rosenberg, M. S., 2004. Wavelet analysis for detecting anisotropy in point patterns.
1082 *Journal of Vegetation Science* 15 (2), 277–284.
1083 URL <http://dx.doi.org/10.1111/j.1654-1103.2004.tb02262.x>
- 1084 Schick, K. D., 1987. Experimentally-derived criteria for assessing hydrologic distur-
1085 bance of archaeological sites. In: Nash, D. T., Petraglia, M. D. (Eds.), Natural for-
1086 mation processes and the archaeological record. Vol. 352 of International Series.
1087 British Archaeological Reports, Oxford, pp. 86–107.
- 1088 Schiffer, M. B., 1987. Formation processes of the archaeological record. University of
1089 New Mexico Press, Albuquerque.
- 1090 Stacey, F. D., Joplin, G., Lindsay, J., 1960. Magnetic anisotropy and fabric of some
1091 foliated rocks from se australia. *Geofisica Pura e Applicata* 47, 30–40.
- 1092 Tarling, D. H., Hrouda, F., 1993. The Magnetic Anisotropy of Rocks. Chapman and
1093 Hall, London.
- 1094 Toots, H., 1965. Orientation and distribution of fossils as environmental indicators. In:
1095 Nineteenth Field Conference of the Wyoming Geological Association. pp. 219–292.

- 1096 Voorhies, M., 1969. Taphonomy and population dynamics of an early Pliocene ver-
1097 tebrate fauna, Knox County, Nebraska. Contributions to Geology, University of
1098 Wyoming Special Paper 1, 1–69.
- 1099 Woodcock, N., Naylor, M., 1983. Randomness testing in three-dimensional orientation
1100 data. Journal of Structural Geology 5 (5), 539 – 548.
- 1101 URL [http://www.sciencedirect.com/science/article/pii/
1102 0191814183900585](http://www.sciencedirect.com/science/article/pii/0191814183900585)